

Protein Engineering

International Edition: DOI: 10.1002/anie.201712448

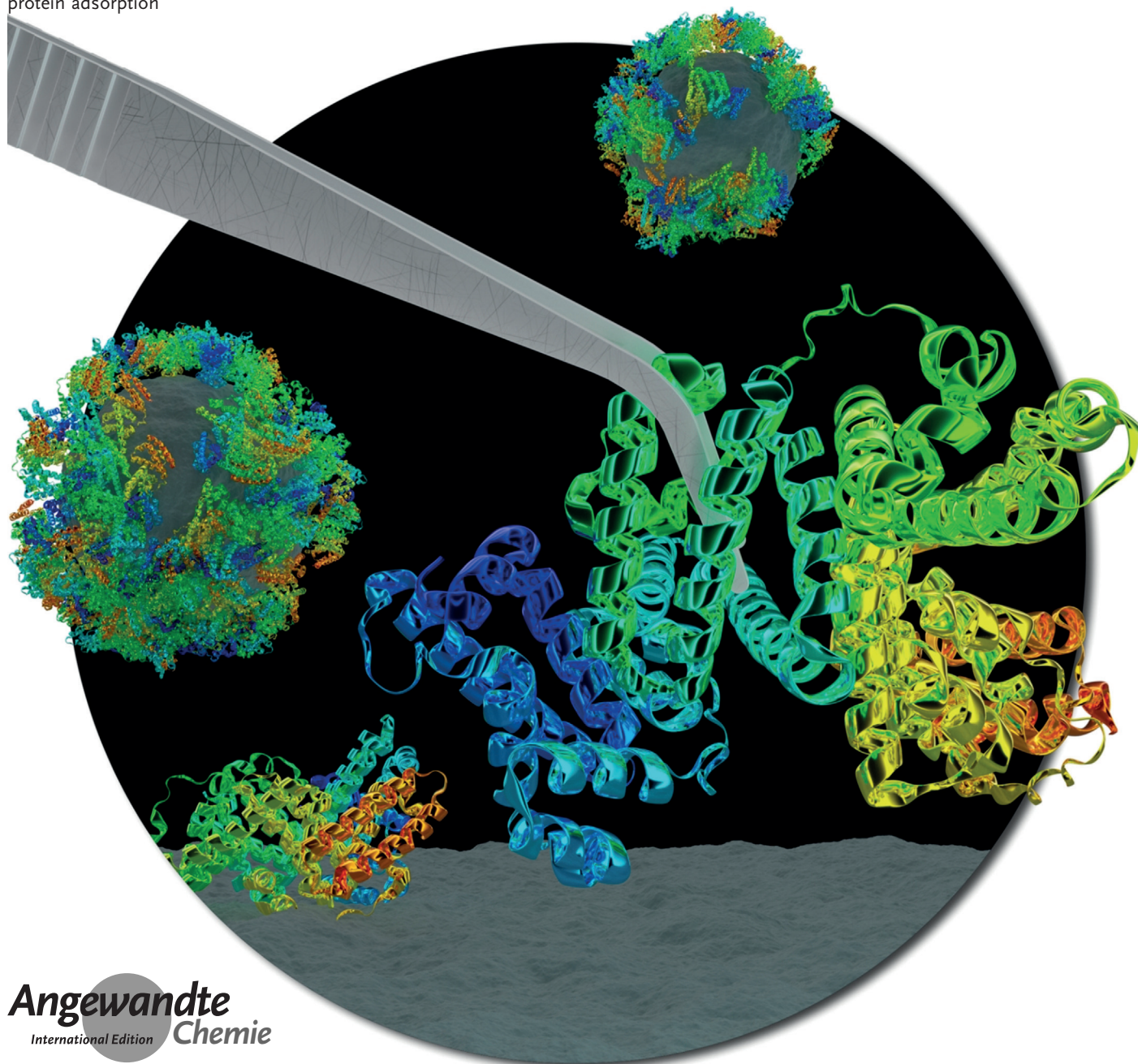
German Edition: DOI: 10.1002/ange.201712448

Engineering Proteins at Interfaces: From Complementary Characterization to Material Surfaces with Designed Functions

*Svenja Morsbach, Grazia Gonella, Volker Mailänder, Seraphine Wegner, Si Wu, Tobias Weidner, Rüdiger Berger, Kaloian Koynov, Doris Vollmer, Noemí Encinas, Seah Ling Kuan, Tristan Berau, Kurt Kremer, Tanja Weil, Mischa Bonn, Hans-Jürgen Butt, and Katharina Landfester**

Keywords:

characterization · engineering ·
interfaces · nanomaterials ·
protein adsorption



Once materials come into contact with a biological fluid containing proteins, proteins are generally—whether desired or not—attracted by the material's surface and adsorb onto it. The aim of this Review is to give an overview of the most commonly used characterization methods employed to gain a better understanding of the adsorption processes on either planar or curved surfaces. We continue to illustrate the benefit of combining different methods to different surface geometries of the material. The thus obtained insight ideally paves the way for engineering functional materials that interact with proteins in a pre-determined manner.

1. Introduction

The field of nanomaterials is growing rapidly. In medicine, tremendous efforts are being made to achieve a successful translation of nanomaterials as carrier systems for diagnostic as well as therapeutic purposes.^[1] Regardless of this purpose, the nanomaterials come into contact with biological fluids and therefore with proteins. These fluids can be either extracellular fluid, such as saliva, mucus, or blood, or intracellular fluid, the cytoplasm. To understand and predict the behavior of nanomaterials in biological systems, it is essential to characterize the interactions between naturally occurring proteins and nanomaterial surfaces.^[2] This is equally relevant for materials outside the medical field where contact with the natural environment cannot be avoided. These are usually planar surfaces such as membranes,^[3] coatings,^[4] or even air–water interfaces,^[5] which naturally also interact with proteins when they are present.

Independent of the material interface and application goal, controlling the interaction of materials with proteins is increasingly seen as a design tool for producing surfaces with a specific function that allows modulation of their properties to improve their efficacy in a biological context. Such control presupposes knowledge of the interaction mechanisms and principles to enable control over the relevant processes, as well as to finally engineer the impact on the desired application. Thus the combination of different techniques to characterize protein–surface interactions goes hand in hand with applying the obtained knowledge to create specific functional systems. In this context, we aim to give a detailed overview of the techniques that are currently applied to characterize and understand the underlying mechanisms of protein interactions at the nanomaterial interface, and show some current directions for engineered protein-repellent surfaces as well as contemporary strategies to obtain functional protein coatings to overcome current challenges for medicinal applications.

2. Analysis Techniques for Proteins at Interfaces


Depending on the type of material being analyzed, different kinds of techniques need to be applied. When proteins interact with curved surfaces such as nanoparticles, the interaction behavior can change compared to completely


From the Contents

1. Introduction	12627
2. Analysis Techniques for Proteins at Interfaces	12627
3. Current Advances and Challenges: From Unspecific to Specific Interactions	12639
4. Summary and Outlook	12644

planar surfaces depending on the protein to nanomaterial size ratio.^[6] However, the most significant change regarding the characterization of planar materials versus nanoparticles is the fact that the nanoparticles are handled as suspensions or dispersions. Thus, for each kind of material, different measurement setups are required. Information on planar surfaces is more easily available by surface-specific techniques ignoring everything that is not present at an interface. For nanoparticles, characterization methods are needed that can either measure the protein–surface interactions in situ or depend on the extraction of the nanoparticles from the biological fluid.^[7] To study these interactions, usually the nanomaterial is incubated in a protein solution first. During the incubation, protein adsorption on the nanomaterial surface takes place until the surface is saturated. The excess proteins will remain in solution and need to be removed from the sample when only the adsorbed proteins are to be characterized. This separation is usually performed by centrifugation and resuspension procedures, where the nanomaterials with higher density will form a pellet. With these washing steps, not only the free proteins but also proteins that are only weakly bound to the surface will be removed so that only the strongly bound, so-called “hard” protein corona

[*] Dr. S. Morsbach, Dr. G. Gonella, Prof. Dr. V. Mailänder, Dr. S. Wegner, Dr. S. Wu, Prof. Dr. T. Weidner, Dr. R. Berger, Dr. K. Koynov, Prof. Dr. D. Vollmer, Dr. N. Encinas, Dr. S. L. Kuan, Dr. T. Bereau, Prof. K. Kremer, Prof. Dr. T. Weil, Prof. Dr. M. Bonn, Prof. Dr. H.-J. Butt, Prof. Dr. K. Landfester
Max Planck Institute for Polymer Research
Ackermannweg 10, 55128 Mainz (Germany)
E-mail: landfester@mpip-mainz.mpg.de
Prof. Dr. V. Mailänder
Department of Dermatology
University Medical Center Johannes Gutenberg-University Mainz
Langenbeckstraße 1, 55131 Mainz (Germany)
Prof. Dr. T. Weidner
Department of Chemistry, Aarhus University
Langelandsgade 140, 8000 Aarhus C (Denmark)

 The ORCID identification number(s) for the author(s) of this article can be found under:
<https://doi.org/10.1002/anie.201712448>.

 © 2018 The Authors. Published by Wiley-VCH Verlag GmbH & Co. KGaA. This is an open access article under the terms of the Creative Commons Attribution-NonCommercial License, which permits use, distribution and reproduction in any medium, provided the original work is properly cited and is not used for commercial purposes.

remains attached to the nanomaterial.^[8] This corona consists of proteins with a high binding affinity and comparably long exchange times in solution. Alternatively, magnetic separation can be used, yielding presumably also some less tightly bound proteins in the corona.^[9] Characterization methods focus on detecting the amount and type of proteins attached to a surface, providing structural information by spectroscopic techniques, and probe protein topography and dynamics. More difficult to analyze is the so-called “soft” protein corona, which represents the weakly associated proteins. The association process of these proteins is considered to take place in the outer layers around a nanoparticle and to be completely reversible.^[8,10] This soft corona consequently produces a different protein pattern to that of the hard corona^[7] and can only be analyzed in the corresponding biological medium without any separation of free proteins. Accordingly, the characterization techniques available are challenging and require in situ measurements. Information can be obtained on size changes, aggregation phenomena, thermodynamics of the adsorption, and viscoelastic properties of the formed protein layers. In principle, the same differentiation can be transferred to planar surfaces where layers of proteins with higher and lower binding affinity are present. Similarly, for the characterization of interactions with proteins, some of the available techniques require the removal of free proteins and/or the surrounding medium while for other techniques, this is not necessary. Usually, protein removal from planar surfaces is achieved by washing steps, which often involve extensive rinsing. Depending on the rinsing conditions also weakly bound proteins might detach again from the interfaces and will not be included in the characterization. Therefore the terms “hard” and “soft” may also be used in terms of protein layers on planar surfaces.

In the following, an overview of the currently established methods for analyzing protein adsorption at different interfaces is given with a differentiation between the kinds of interaction (weak or strong) that are accessible. In addition, the possibilities of tackling protein structural questions with computer simulations are briefly discussed.

2.1. Characterization of High-Affinity Proteins

2.1.1. Protein Quantification Assays

To quantify the adsorbed protein amount on both nanomaterials and planar surfaces, protein assays are probably the

most used and most straightforward way to characterize protein interactions.^[11] The basic principle of all assay types relies on the direct interaction or reaction between certain functional groups of the proteins and a reagent that subsequently produces a color change proportional to the protein concentration. For nanomaterials, protein quantification assays have been established where after adsorption and several washing steps the remaining protein amount is analyzed. The same can be done for planar surfaces with different washing techniques. The only drawback compared to nanomaterials is the much lower surface area so that higher assay sensitivity is needed. Once the not-so-stringently bound proteins and the supernatant have been washed away, quantitative desorption of the proteins from the nanoparticle surface is needed. This is ensured by using denaturing conditions such as heat and urea and/or solubilization by detergents such as CHAPS (3-((3-cholamidopropyl)dimethylammonio)-1-propanesulfonate)^[12] or sodium dodecyl sulfate (SDS).^[13] Nearly all studies aimed at determining protein adsorption assume that they have removed the bound proteins entirely. The surfactants employed regularly are used at high concentrations and can disturb the determination of the total amount of desorbed protein.^[14] Additionally, the influence of the removal of the detergents by specific columns has not been investigated in this setup. That said, nearly all groups determine the total protein content by a colorimetric assay, such as the Lowry,^[15] Bradford,^[16] or BCA (bicinchoninic acid)^[17] assay or others. The method after Bradford is based on the Coomassie stain and depends on the amount of nonpolar and cationic side groups of the proteins. BCA-based tests are thought to be more resistant to surfactants than Bradford assays. Aside from the fact that they need to be resistant to the detergents used, their reliability when determining the total amount of different protein mixtures is also complex. Whereas the result of a Bradford assay depends on the number of nonpolar and cationic side groups of the proteins, BCA-based assays depend on the Biuret reaction and thus the interaction with acidic side groups. With a complex mixture of proteins, the differences in the detection mechanisms should be leveled out, but when the proteome detected becomes less and less complex, recalibration with the most abundant protein is advised.



Svenja Morsbach obtained her diploma in Biomedical Chemistry from the Johannes Gutenberg University of Mainz in 2012. For her PhD thesis, she joined the group of Katharina Landfester at the Max Planck Institute for Polymer Research. Her thesis, which she completed in 2015, focused on the interaction between polymeric nanomaterials and blood plasma proteins. Since 2015, she has been a group leader in the same department, being responsible for the Polymer Analysis Group and continuing in the same research field.



Katharina Landfester first accepted a professorship for Macromolecular Chemistry at the University of Ulm in 2003 after obtaining her habilitation at the University of Potsdam. Since 2008, she has been a director at the Max Planck Institute for Polymer Research in Mainz where she focuses on the establishment of functional colloidal systems, especially in the field of drug delivery.

2.1.2. Gel Electrophoresis

To determine the composition of proteins forming the hard protein corona, desorbed proteins can be separated electrophoretically by so-called sodium dodecyl sulfate polyacrylamide gel electrophoresis (SDS-PAGE).^[18] Proteins are denatured by the addition of SDS in large amounts and heating up to 95°C. This procedure transforms them into elongated, uniformly charged polymers. Furthermore, reducing agents such as dithiothreitol (DTT) can be used to cleave disulfide bonds within proteins or ones linking two proteins or peptides together. In this way, any subunits that might be present will be separated. The electrophoretic mobility of such SDS-solubilized proteins depends only on the length of the protein as the number of attached anionic SDS molecules is proportional to the number of amino acids in the chain. The meshwork of the gel then provides a preformed obstacle and thus the movement of longer protein chains is more hindered than that of shorter ones. The density of the meshwork determines the range of protein chain lengths that can be conveniently separated. Known protein standards run in the same polyacrylamide gel electrophoresis (PAGE) give information on the size of the other protein bands in the samples. To visualize the bands, a staining method needs to be employed. Coomassie blue is most widely used because it is inexpensive.^[19] Other methods such as fluorescence^[20] or silver staining^[21] have a higher sensitivity, and for fluorescent stains, a better linearity over three to four log units is achieved.

Albeit a simple method, a 1D SDS gel gives a good picture of the complexity of the proteins, and with some knowledge with regard to the expected proteins, this analysis provides guidance to further analysis methods to be performed. In addition, by transferring the proteins to a nitrocellulose membrane by electroblotting or just soaking the proteins through the gel towards a nitrocellulose membrane, a classical Western blot can be performed.^[22] Here, proteins of interest are detected with a combination of a primary and secondary antibody, with the latter being coupled to an enzyme that stains the nitrocellulose membrane at the specific site when an appropriate substrate is added. In this way, proteins of very low abundance can be detected and even quantified relative to the amount of the same protein in other samples.

Analysis is more tedious and laborious when a second dimension is added to the SDS PAGE. This is mostly done by separating the proteins according to their isoelectric point first in a 1D gel in a strip (isoelectric focusing).^[23] By then fitting this strip to an SDS PAGE and running the second dimension, many more proteins spots can be detected.^[24] Here, the identification is getting more complex with regard to clear determination of the proteins depicted on the gel pattern. The added dimension of isoelectric points separates isoforms and differentially glycosylated species of the same protein more distinctly. With this added complexity comes the need for a highly reproducible sample and gel preparation procedure in order to compare results. Even when the gels are run in the same chamber in parallel, direct comparison, one first needs to realign the protein spots. This is done usually

with the help of computer programs.^[25] Still, only relative results can be obtained by 2D gel electrophoresis.

To determine which protein exactly is representing the spot on a 2D gel, a further determination of the protein needs to be performed. Here, mass spectrometry has been established and is currently the gold standard.

2.1.3. Mass Spectrometry (MS) and Liquid Chromatography Coupled with Mass Spectrometry (LC-MS)

To identify the protein of a specific spot on an SDS PAGE or a 2D SDS PAGE gel, mass spectrometry has been the most versatile method.^[26] This method requires that a large number of spots are picked, the proteins in the spots are digested to small peptides, and then the peptides are ionized and identified in a mass spectrometer. The interesting aspect of the mass spectrometer here is that not only the mass of the whole peptide is determined. For a short time, the mass spectrometer is switched into collision mode and back again. During operation in the collision mode, the peptide is broken into pieces along its backbone, also at the peptide bond. The daughter ions represent all the N-terminal and C-terminal parts of the peptide to the left and right side of the broken bond. Hereby, the amino acid sequence can be reconstructed. Once protein spots have been identified on one gel and if the alignment of other gels is sufficient, spots on other gels can be assigned to certain proteins.^[25] If there are even slight doubts whether two spots on two gels should be assigned to the same protein, protein identification with MS needs to be repeated. Although digestion and MS workup can be automated and with autosamplers also the loading of the samples into the MS is simplified, it remains to be a tedious method rarely defining more than a few hundred spots.

Here, the coupling of a separation technique directly to a mass spectrometry device was an enormous step forward. Liquid chromatography (LC) is the method of choice to be coupled to mass spectrometry (LC-MS).^[27] Unlike in the SDS-PAGE-MS setup, in the LC-MS workflow, instead of identifying whole proteins, all proteins in a sample are digested into peptides before the separation.^[28] Only afterwards, the peptides are separated by liquid chromatography. The amino acid sequence of the different peptides is then determined by considering the masses of the mother and daughter ions as detailed above. The daughter ions provide the forward and backward sequencing of the peptides. Then the found peptides are matched to the amino acid sequence of all known proteins of a species. This is much more complex than the identification of one protein but can be done by the use of software packages. As a result, also complex samples such as plasma with several hundreds or thousands of proteins or less complex samples such as the protein coronas of nanocarriers can be identified in a single run. As not only the masses of the peptides are known but also how many peptide ions (mother or daughter ions) were detected in the mass spectrometer, the amount of a certain protein can be quantified by averaging the three most abundant peptides of this protein.^[29] With this, relative comparisons can be done, or, if the absolute total amount of proteins has been determined, also absolute quantifications are possible (Fig-

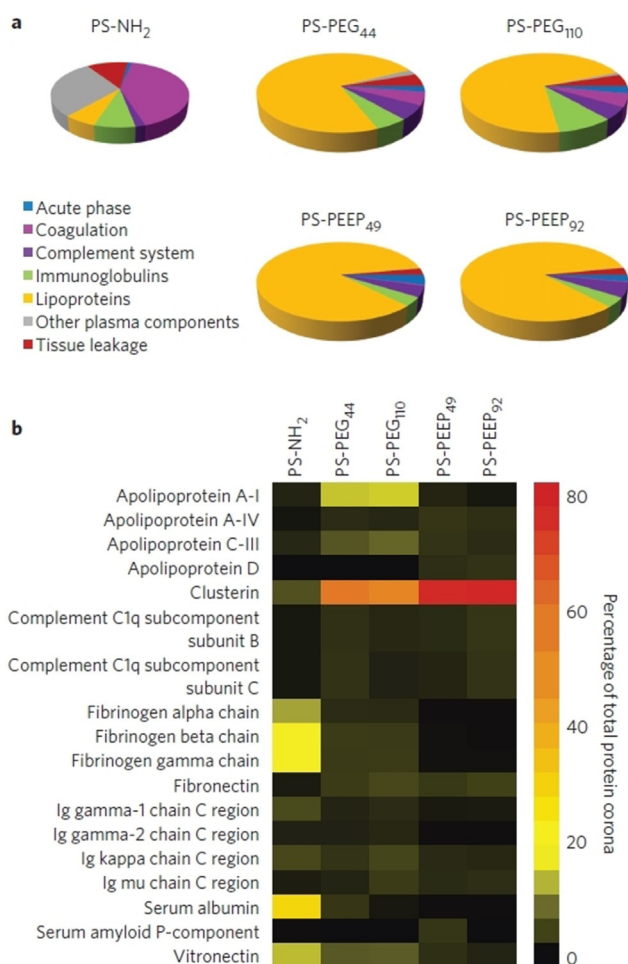


Figure 1. a) Proteins identified by quantitative mass spectrometry are clustered into groups to give an overview. b) Heat maps are an appropriate help for visualizing the amount of single proteins across different conditions. Figure reproduced from Ref. [13].

ure 1b). With several hundreds or sometimes thousands of proteins identified, grouping of proteins into functional groups is necessary (Figure 1a).

One challenge in proteomics was that the sample amount is usually low. Because of the needs in biology and medicine, dead volume and separation columns were reduced in size.^[30] With higher pressures and the use of electrospray ionization, now ten thousands of peptides can be identified in a 60 to 120 minute run, with multitudes of spectra being needed for the identification of one peptide. The challenge of converting MS spectra into peptides and then assigning these peptides to proteins has been accomplished through the use of bioinformatic tools and is now involving the highly parallel use of graphic processors to speed up the identification process.

While all of these technological challenges have been mastered in the last decades, sample preparation and data interpretation are crucial for further development. This begins with the protein source used for the investigations.^[31] Native blood and plasma cannot be stored and handled outside the living body. Blood either needs the addition of an anticoagulant such as heparin or a calcium chelator or the

proteins of the coagulation have to be removed. The latter is achieved by activating the coagulation cascade. The clot formed out of fibrinogen removes these proteins. The end product is then called serum. Either of these changes—removing the coagulation cascade by making serum or the anticoagulation of plasma—results in a different protein corona.^[31] This demonstrates the need for exact descriptions of the experimental procedures in all publications.

2.1.4. Sum Frequency and Second Harmonic Generation (SFG and SHG)

Besides the quantitative ex situ techniques mentioned so far, even-order nonlinear optical (NLO) spectroscopies have emerged as in situ probes of ordering and conformation of proteins at interfaces. The main advantages of these NLO spectroscopies over linear spectroscopies are their intrinsic surface specificity and monolayer sensitivity.

More than 100 000 protein structures are available in the protein database (PDB). Yet, not a single protein structure on a solid surface has been reported. The reason for our lack of insight into the structure and ordering of interfacial proteins can be traced back to the challenges involved in probing the extremely small amounts of proteins present at a surface. In this respect, nonlinear optical surface-specific spectroscopies that selectively sample the solid/liquid interface are a promising approach. Specifically, sum frequency and second harmonic generation (SFG and SHG) have become reliable tools that provide surface-specific information on proteins at interfaces. SFG and SHG owe their surface specificity to the selection rule that symmetry must be broken, which evidently applies at the phase boundary between two media.^[32] For the past ten years, researchers in this field have been developing methods to obtain molecular-level pictures of protein structures at surfaces. The most important questions and challenges that these methods address are summarized in Figure 2: How is a protein folded on the surface and what is its orientation? Which side chains are interacting with the surface? How is the surface structured and how does hydration change in the presence of proteins? What are the roles of refolding, structural dynamics, and the flow of energy across proteins at the surface?

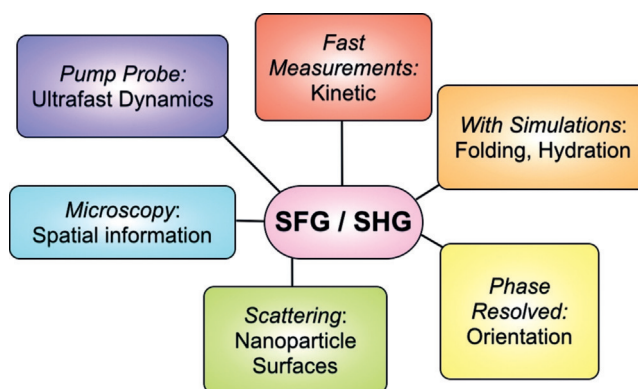


Figure 2. Different nonlinear optical spectroscopy methods provide access to different aspects of protein–surface interactions.

In an SFG experiment, infrared (IR) and visible (Vis) laser pulses are overlapped in time and space at a surface (see Figure 3a), leading to the generation of photons at the sum frequency of the IR and Vis frequencies (inset in Figure 3a).

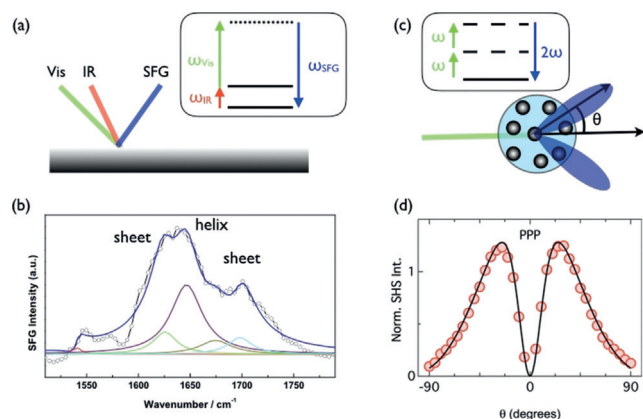


Figure 3. Schematic representation of nonlinear optical experiments. a) SFG spectroscopy (side view) in reflection geometry. Vis and IR beams are overlapped to detect a surface vibrational spectrum. Inset: level diagram (continuous/dotted lines indicate a real/virtual state). b) SFG spectra in the amide I region can be used to identify the folding and orientation of proteins at surfaces. The spectra show the amide I signal of the B1 domain of protein G bound to a UV-treated polystyrene surface. The helix and sheet signals related to the protein secondary structure show that the protein is in a near-native state. Amide I spectra collected with different laser polarizations can be used to determine the orientation of the folding motifs. c) Second harmonic generation from the surface of an ensemble of nanoparticles in scattering geometry (SHS, top view): As the detection arm rotates in the horizontal plane, different conditions of constructive and destructive interference are met. Inset: level diagram (the continuous line indicates a real state while dashed lines indicate states that can be either real or virtual). d) Example of an SHS scattering pattern: SHS intensity vs. scattering angle (red symbols: experimental data; black line: best fit) from hexanol-covered hexadecane oil droplets ($R = 75$ nm). $\theta = 0$ indicates the propagation direction of the fundamental beam. Modified from Ref. [33] with permission. Copyright 2016 American Chemical Society.

Vibrational information is obtained when the IR frequency is resonant with a vibrational mode (Figure 3b), where the IR frequency is tuned in the amide I region that reports on the protein secondary structure. All amide regions are conformation-sensitive and have specific signatures for α -helix, β -sheet, and loop structures, and the complex spectrum reflects the presence of different protein substructures at the surface. SHG is the degenerate case of SFG when only one laser beam is used and frequency-doubled photons are generated as shown in the inset of Figure 3c. Information on electronic transitions can be obtained from SHG when either fundamental or the emitted frequency-doubled photons are resonant with an electronic transition.

Nonplanar surfaces, such as the surfaces of nanoparticles, can be probed in scattering geometry^[34] by second harmonic scattering or sum frequency scattering (SFS and SHS, respectively), as shown in Figure 3c. Similar to linear light scattering, a scattering pattern will appear as shown in Figure 3d that depends on particle size, shape, composition,^[35]

and surface charge^[33,36] as well as the nonlinear optical response from the proteins located at the surface, the information of interest. SHG from planar interfaces has previously been employed to study proteins at the air/water interface^[37] and those interacting with a membrane.^[38]

Detailed reviews on SFG and SHG can be found in Ref. [39]. Pioneering studies based on SHG^[40] and SFG^[41] have reported on amino acids at the air/water and oil/water interface, respectively, which has paved the way for label-free studies of protein structure and interfacial protein hydration by these two techniques.^[42] SFG can now determine all key aspects of protein surface structures, namely the side chain structure,^[43] orientation, and backbone folding.^[44] The orientation of side chains can be determined by labeling individual side chains with deuterium.^[45] This strategy has been developed using amphiphilic LK peptides as model systems. LK peptides are composed of only two types of amino acids, hydrophobic leucine (L) and hydrophilic lysine (K). Depending on the amino acid sequence, α -helix, 3_{10} -helix, and β -sheet structures can be obtained, and therefore, these peptides have served as model systems to develop SFG methods to obtain information on surface-binding leucine sites by making use of deuterium-labeled side chain structures.^[46] The secondary structure of interfacial proteins and information on changes in protein conformation at interfaces can be obtained by SFG in the amide regions. Complex biomolecules such as synthetic peptides or natural proteins on biologically relevant interfaces have been probed through their characteristic amide I signals,^[47] sometimes accompanied by chiral measurements of the N–H stretch,^[48] and the amide III signal.^[49] The amide regions of such spectra can also be used to determine the orientation of proteins by comparing peak ratios from spectra obtained using different laser polarizations. The Chen group has developed several successful models in this context.^[50]

As the methods described above rely on direct spectral assignments of amide modes based on published IR peak positions, the analysis is limited to smaller proteins and peptides with clear folding motifs. This difficulty of studying large proteins is also well known in the IR field, and is further complicated by the coherent nature of the SFG signal and the resulting interferences between resonant modes. To make full use of the complexity of SFG amide spectra, several groups have developed theories to directly calculate SFG spectra from simulated structures.^[50a,b,51] This combination of theory and experiment has enabled the study of very large proteins on complex surfaces. This has led, for instance, to a major advance in the understanding of the biogenesis and maintenance of thylakoid membranes by showing how the IM30 protein, shown in Figure 4, is oriented at the membrane surface to trigger membrane fusion in cyanobacteria and chloroplasts.^[52]

The next challenge in the field will be the observation of protein motions and dynamics. A very first step in this direction has been the execution of sub-picosecond time-resolved SFG experiments to directly quantify the reorientation of an amino acid side chain at an interface^[53] and the energy transfer within the hydration shell of ice-nucleating bacteria.^[54] Future developments will be directed towards the

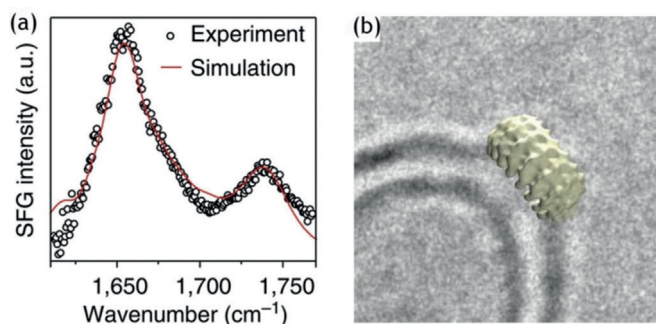


Figure 4. a) Experimental (circles) and calculated (line) SFG spectra in the amide I region of IM30 bound to a model MGDG/PG monolayer at the air–water interface. The calculated spectra match the experimental data well for upright monomer orientations. b) 3D reconstruction in an isosurface view. Note that the 3D reconstruction matches the extra electron density in size and shape, indicating perpendicular binding of IM30 to the membrane surface. Modified from Ref. [52] with permission. Copyright 2015 Nature Publishing Group.

observation of protein backbone motions, reorientation, and biochemical reactions.

Finally, protein adsorption on highly curved surfaces is, in many instances, more relevant than adsorption on planar surfaces. One advantage of SHG and SFG is that these methods do not necessarily require planar interfaces; in fact, they can be carried out in scattering mode, thus allowing the observation of interactions of molecules with nanoparticles in solution.^[34,55] Promising results in this direction have been obtained by both SHS and SFS.^[56] Recent advances in theory and scattering experiments have also enabled the study of soft particles such as liposomes and droplets, and show great potential in understanding the influence of charged surfaces on protein adsorption on NPs.^[33,36c]

2.1.5. Fourier Transform Infrared (FT-IR) and Circular Dichroism (CD) Spectroscopy

As SFG and SHG are not yet routinely applied to nanoparticles, simpler spectroscopic techniques such as FT-IR and CD spectroscopy are currently the state of the art to determine the structure of proteins that are bound on curved surfaces of nanocarriers in solution.^[57] Both techniques are sensitive to the secondary structure of the protein and currently the only ones that are regularly used to judge protein denaturation upon adsorption. With FT-IR, the absorption of the sample in the IR range (typically, wavenumbers of 1800 cm^{-1} to 1300 cm^{-1}) is analyzed, where the amide bands are specific for structural elements such as α -helices and β -sheets.^[57,58] In particular the “amide I band”, representing the C=O stretching motion of the amide groups at 1600–1700 cm^{-1} , is sensitive to the secondary structure because of potential hydrogen bonding and dipole interactions. CD spectroscopy makes use of the different adsorption of left and right circularly polarized light and the chirality of proteins and is applied in the UV range (180–320 nm).^[57,59] Similarly, the different contributions of the typical amide group adsorption again provide information on the overall amount of α -helix, β -sheet, and unordered structural ele-

ments. Both techniques can in principle be applied to measure the hard and soft protein corona, meaning that the free proteins do not necessarily need to be removed from the nanocarriers. However, when free proteins are not removed, the obtained signal will be an average over the whole sample and thus result from free and adsorbed proteins at the same time. This means that the only accessible information is that a change in the protein structure did or did not occur but no quantification of structural changes is possible. In addition, very subtle changes might not be visible with this procedure. Removing the free proteins allows analyzing only the proteins with a high binding affinity, which also brings some difficulties. After washing, the protein/nanocarrier ratio is significantly decreased, which potentially results in insufficient sensitivity (because of the low protein concentration) or high sample turbidity (owing to the high nanomaterial concentration). Turbid samples are not suitable for CD spectroscopy measurements as the polarized light still needs to pass through the sample. Another problem is the absorption of additional components other than proteins in the sample when working in aqueous environments. For example, some buffers containing chloride or Tris also absorb light in the UV range so that the buffer system for the samples must be carefully chosen. Especially for physiological media, those are not the optimum sample conditions. All of those disadvantages make clear that both techniques were not originally designed to analyze proteins in the presence of other materials such as nanocarriers. For the advancement of the field, new methods are needed that tolerate high nanocarrier concentrations and the presence of other small molecules.

2.1.6. X-ray Photoelectron Spectroscopy (XPS) and Time-of-Flight Secondary Ion Mass Spectrometry (ToF-SIMS)

X-ray photoelectron spectroscopy (XPS) and time-of-flight secondary ion mass spectrometry (ToF-SIMS) have been developed into reliable tools to probe interfacial proteins.^[60] For an XPS experiment, the sample is placed in ultrahigh vacuum and irradiated with X-rays.^[39c,61] The emitted photoelectrons provide information on the elemental composition, chemical state, and surface concentration from within the top 10 nm of the surface. The chemical specificity of XPS allows for the detection of adsorbed organic layers on planar, but also nanoparticle surfaces^[62] by tracking a distinctive element of the protein structure (normally nitrogen) or the attenuation of a surface element signal.^[63] Although depth profiling^[64] and imaging are also feasible by XPS, a limitation on spatial resolution due to X-ray focusing without inducing sample damage still has to be overcome.^[65] A spatial resolution of up to 0.1 μm and depth profiling of 1–2 nm can be achieved. An ion beam is focused on the surface, which then ejects secondary ions and clusters that generate a mass spectrum surveying molecular fragments with atomic masses of 0–10000. ToF-SIMS provides information on the composition, structure, and conformation of complex protein layers on planar surfaces with high sensitivity and specificity (10^7 – 10^{11} atoms cm^{-2}). This is achieved by bombarding a surface with a focused ion beam, inducing the emission of secondary ions whose masses are determined when reaching the

detector, considering that ions with different masses but the same energy travel with different velocities.^[66] The combination of both techniques effectively probes the orientation, secondary structure, binding chemistry, and side-chain geometry of surface-bound proteins, therefore aiding the development of new biomaterials.^[60,67]

2.1.7. Scanning Force Microscopy (SFM)

Sample surfaces can be imaged and characterized in situ, that is, in the natural aqueous environment of proteins, with scanning force microscopy (SFM) methods. Thus the specific function of the proteins can be maintained. Most commonly, SFM is used to record topographic images of solid surfaces. The underlying working principle of SFM is based on scanning sample surfaces with a sharp tip, which is situated at the end of a cantilever spring (Figure 5a). While scanning, the force between the tip and the sample is measured by monitoring the deflection of the cantilever. An electronic feedback loop is then used to adjust the tip-sample distance to maintain a constant tip-sample force at each pixel of an image. Thereby a contour map of the surface topography is recorded without destroying it. In general, the lateral resolution that can be obtained depends on the conditions of the sample, the geometry of the SFM tip apex, and the interaction between the two. In some cases, atomic resolution is achieved for planar samples such as calcite in liquids.^[68] More typical for applications in soft matter science is a lateral resolution of 1–10 nm. Here, we highlight SFM as a tool to probe a) single protein recognition events, b) the distribution of proteins on surfaces, and c) the activity of protein dynamics.

a) Binding partners can be specifically recognized by molecular force spectroscopy. Hereby one of the binding

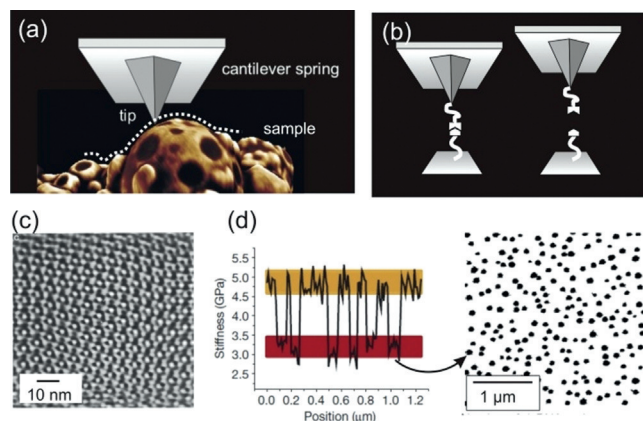


Figure 5. a) Schematic representation of a sharp tip that is scanned over a sample consisting of patchy colloids.^[69] b) Single-molecule force spectroscopy to probe the unbinding of specific molecules. Retraction of the tip leads to rupture of the bond. c) Atomically resolved structure of bacteriorhodopsin adsorbed to mica. Reprinted from Ref. [70] with permission from Elsevier. d) Left: Hybridized DNA molecules were measured to be less stiff than single-stranded DNA. The stiffness difference has a binary character. Right: The binarized stiffness values (black areas) correspond to areas with double-stranded DNA. Reprinted with permission from Ref. [71].

partners is immobilized on the tip and the other on the sample surface. When the tip is brought close to the sample surface, both binding partners interact. This interaction can be probed by measuring the force upon retraction of the tip (Figure 5b). This method has been used to probe the potential landscape upon unfolding of proteins,^[72] and it can be used to probe the presence of hydrogen bonds between binding partners.^[73]

b) The lateral distribution of proteins can be measured in the topography mode. More than two decades ago, the membrane protein bacteriorhodopsin adsorbed to mica in buffer solution has been imaged (Figure 5c).^[70] Meanwhile the electronics of the SFM method have been improved, allowing for routine investigations of native membrane proteins such as ion-driven rotors.^[74] By combining the topography imaging mode with force spectroscopy techniques, local information about the protein distribution can be obtained. For example, Preiner and co-workers used such a combined method with a biotinylated IgG-functionalized tip to resolve single avidin molecules locally immobilized on mica.^[75] Husale and co-workers investigated the nanomechanical response of DNA molecules and extracted differences in the molecular stiffness between single-stranded and double-stranded DNA molecules (Figure 5d).^[71] These examples highlight that SFM is a valuable tool also to investigate the lateral distribution of functional proteins at interfaces.

c) A more compact and careful design of SFM components allows increasing the imaging speed up to video rate (30 frames per second).^[76] Video-rate imaging allows following the dynamics of proteins in real time.^[76c] A prominent example is the molecular motor motion dynamics of myosin V walking along an actin filament.^[77]

For future developments, it is worth noting that SFM is a tool that can probe a variety of tip-surface interactions going beyond topography imaging. For example, magnetic and electrostatic imaging modes can be readily used in aqueous solutions. This may allow analyzing charge transport or studying the influence of charges on specific protein structures or functions. However, liquid electrostatic imaging depends strongly on the environmental conditions, such as ionic strength, leading to screening of charges. Screening constitutes an obstacle to study charges of molecules with atomic resolution. However, in air, charge propagation along individual pili proteins was probed using electrostatic force microscopy.^[78]

2.2. Characterization Including Low-Affinity Proteins

2.2.1. Dynamic Light Scattering (DLS)

DLS is currently often used as a quick method to determine size changes of nanomaterials before and after contact with protein solutions. Usually this is done to confirm the development of a protein layer (corona) around the nanomaterial and further to estimate the layer thickness.^[79] To determine the size or size increase of an object in solution, in DLS, the intensity fluctuation of the light scattered from diffusing species in the sample at a given angle is recorded. This count rate trace will then be converted into an autocorrelation function $g_1(t)$ (see Figure 7 for examples),

Table 1: Overview of methods used for characterizing high-affinity proteins.

Method	Accessible protein sources	Available information
Protein quantification assays	Protein mixtures/ single proteins	Protein amount
Gel electrophoresis	Protein mixtures	Protein pattern/identification
Liquid chromatography mass spectrometry (LC-MS)	Protein mixtures	Protein pattern/identification
Fourier transform infrared (FT-IR)/ circular dichroism (CD) spectroscopy	Single proteins	Protein secondary structure on nanoparticles
Sum frequency generation (SFG)/ second harmonic generation (SHG)	Single proteins	Protein secondary structure, orientation, hydration
X-ray photoelectron spectroscopy (XPS)/ Time-of-flight secondary ion mass spectrometry (ToF-SIMS)	Protein mixtures/ single proteins	Protein amount, secondary structure on flat surfaces, orientation
Scanning force microscopy (SFM)	Protein mixtures/ single proteins	Single protein interaction forces, surface topography, dynamics of proteins

describing the “self-similarity” of the count rate trace. Smaller objects will diffuse very quickly, causing fast fluctuations of the interference pattern coming from scattered light and thus result in a low self-similarity, that is, an autocorrelation function with a short relaxation time. Larger objects, in contrast, result in long relaxation times owing to the slow diffusion and associated interference pattern fluctuation. The autocorrelation function can then be fitted by various different algorithms to yield the diffusion coefficient(s) that can be detected. As this diffusion coefficient can depend on the scattering angle, it can be determined for several angles and afterwards extrapolated to zero. Conversion into the hydrodynamic radius is then achieved by the Stokes–Einstein equation.

In many studies, the protein layer thickness is investigated with single-angle light scattering devices, which provide exact values only for very small particles or monodisperse large particles. Also, the values are obtained by averaging over the whole solution, ignoring the presence of polydispersity. This means that if the sample preparation and measurements are not carried out carefully, the data can easily be overinterpreted. This problem has been discussed in great detail lately by Schmidt and co-workers, who pointed out the challenges of applying DLS especially in the area of nanomedicine.^[80] To be able to give precise information on size changes of a nanomaterial, multiangle DLS should be performed, and special attention has to be paid to the sample preparation and data interpretation. For well-defined systems, it can be possible to not only describe the overall size change but to obtain the protein adsorption isotherms by varying the protein concentration.^[81] This is, however, only possible for small particles and very reproducible measurements. The determination of the thickness of a protein layer becomes more and more unprecise for larger nanocarrier systems. The method of DLS becomes less accurate for particles with an R_h larger than 100 nm, and thus the error significantly increases. In that size range, protein layers of only a few nanometers in thickness

cannot be detected anymore because of the experimental error.

The analysis can even become much more complicated when mixtures of proteins are considered as the interacting protein source. In some cases, this problem is solved by removing free proteins from the solution before the measurement. However, this always means that the remaining proteins will be “diluted” and can detach from the nanoparticle surfaces over time as long as the process is reversible. Thus this scenario is not a very close representation of true biological environments. To tackle this challenge, Schmidt et al. developed a method to determine size changes and aggregate formation in complex mixtures such as nanoparticles in concentrated blood plasma or serum (Figure 6).^[82] This method allows considering multiple diffusing species as background (such as the pure plasma and nanocarrier components) and searching for “newly” formed species of different sizes that were not detected before. The most significant advantage of this technique is that the nanomaterial and its adsorbed proteins can be characterized directly in the corresponding medium, and free proteins do not need to be removed. However, aggregates or species of larger size will always be analyzed with regard to their intensity contribution so that their true concentration (number average) can be overestimated. Thus the most meaningful information that can be obtained for a system is the fact that no large aggregates can be detected and that all size changes remain within the experimental error. This information can be used a quality control step, and as such DLS has been applied successfully.^[83]

As the technique is based on measuring the Brownian motion of species in solution, it cannot be applied to interaction of proteins with planar surfaces.

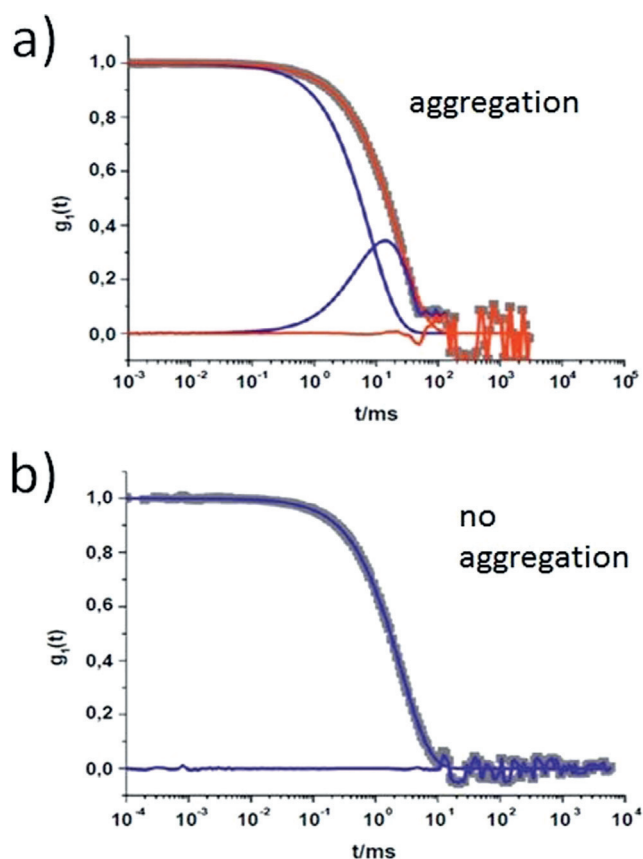


Figure 6. The complex analysis of dynamic light scattering measurements in concentrated human serum with a method after Schmidt et al.: Autocorrelation functions $g_1(t)$ for a scattering angle of 60° and corresponding fits together with the resulting residuals of a) unfunctionalized polystyrene nanoparticles yielding newly formed aggregates in human serum and b) carboxy-functionalized polystyrene nanoparticles exhibiting no size changes in the mixture. The blue lines represent the fits corresponding to the sum of the individual plasma and nanocarrier components. The red line represents the sum of the individual components together with an additional term for aggregates. Extracted and adapted from Ref. [84].

2.2.2. Fluorescence Correlation Spectroscopy (FCS)

FCS is a powerful tool for investigating the mobility of fluorescent species, such as small molecules, macromolecules, or nanoparticles, in various environments. The technique is based on monitoring the fluctuations of fluorescence light originating from species diffusing through a very small ($< 1 \mu\text{m}^3$) observation volume, commonly created in confocal microscopy configuration. The Brownian diffusion of the fluorescent species in and out of the observation volume creates time-dependent fluctuations in the detected fluorescent intensity $\delta I(t)$. These fluctuations are recorded and evaluated in terms of an autocorrelation function $G(\tau) = 1 + \langle \delta I(t)\delta I(t+\tau) \rangle / \langle I(t) \rangle^2$ (Figure 7b). Finally, a fit with an appropriate model equation yields information on the diffusion coefficient and the hydrodynamic radius of the studied species, their concentration, fluorescence brightness, etc.^[85] While first developed and still mostly used in molecular

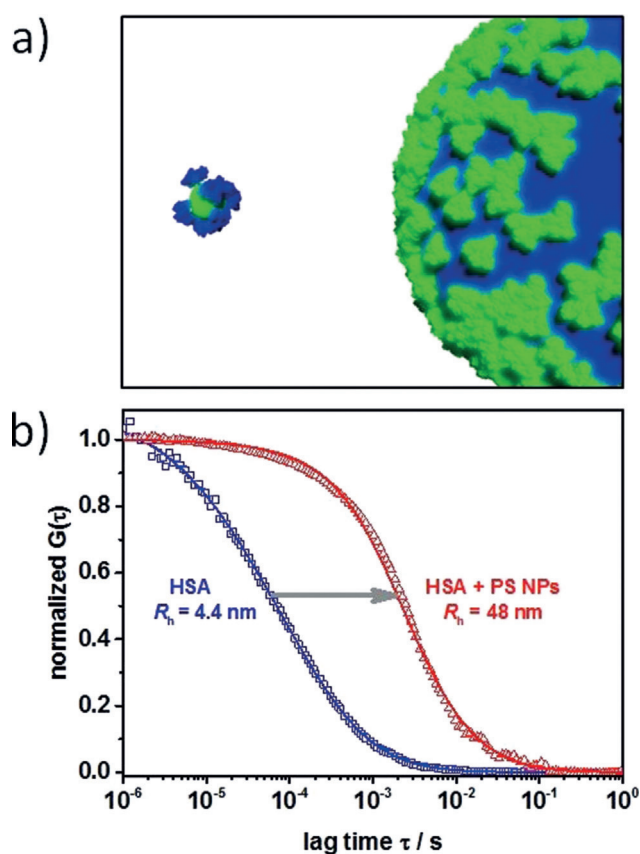


Figure 7. a) To-scale drawing of a 10 nm diameter nanoparticle surrounded by albumin and a 100 nm diameter nanoparticle surrounded by albumin. The fluorescent species is in each case indicated in green, the non-fluorescent one in blue. b) Normalized FCS autocorrelation curves measured for fluorescently labeled HSA in the absence (squares) and presence (triangles) of 100 nm diameter non-fluorescent polystyrene nanoparticles. The arrow indicates the strong shift to smaller diffusion coefficients for proteins adsorbed on the NPs.

and cell biology,^[86] in the last decades, FCS has found many applications in polymer, colloid, and interface science.^[87]

FCS can provide important insight into protein corona formation and can be used complementary to DLS. The main difference between DLS and FCS is that FCS is based on fluorescence detection. Thus fluorescent labeling of the studied nanoparticles or proteins may be necessary. This can be considered as a certain disadvantage although fluorescent labeling protocols are well established nowadays, and various fluorescent nanoparticles and proteins are commercially available. On the other hand, the fluorescence detection is also the main advantage of FCS as it is the reason for the very high sensitivity and selectivity of this technique, which makes it particularly suited to study protein–nanoparticle interactions under both model (e.g., protein solutions) and physiological (e.g., blood serum) conditions. Only very low concentrations of labeled species are required. Here, two main approaches can be considered, as schematically shown in Figure 7a.

If the protein corona is large compared to the bare nanoparticles, its formation can be studied using fluorescent nanoparticles and non-labeled proteins. One measures the

increase in the nanoparticle's hydrodynamic radius upon protein adsorption. Good examples for such studies are the works of Nienhaus and co-workers^[88] and Mukhopadhyay and co-workers,^[89] who used fluorescently labeled FePt nanoparticles, quantum dots, or gold nanoparticles to study the adsorption of non-labeled proteins with FCS. Because of the very small size of the studied nanoparticles (ca. 10 nm) both groups were able to detect the formation of even a single monolayer of proteins on the nanoparticle surface. The FCS studies allowed an estimation of the equilibrium dissociation coefficients and provided information on the orientation of the adsorbed protein molecules. While these studies were performed with solutions containing only one type of protein, recently, Nienhaus and co-workers^[90] have extended them to a complex biofluid, human blood serum, where the fluorescence-based selectivity of the FCS may be particularly useful. Indeed, the presence of larger species or aggregates in undiluted biofluids can complicate DLS experiments as discussed in the previous paragraph. As FCS "sees" only the fluorescent nanoparticles, it may provide more valuable insight, such as whether the nanoparticles have been incorporated into aggregates and, if so, how many nanoparticles are found per aggregate.

If the studied nanoparticles are significantly larger than the protein molecules (Figure 8A), which is commonly the

case when drug nanocarriers are considered, the increase in the hydrodynamic radius of the nanoparticle upon protein adsorption is too small to be detected by DLS or FCS. In such situations, the only sensitive enough experimental approach is the use of FCS and fluorescently labeled proteins.^[8a,91] Because of the selectivity of the technique, the binding of even a single fluorescent protein to a non-fluorescent (at the same excitation wavelength) nanoparticle is manifested by a strong increase in the measured R_h and can be easily detected (Figure 7B). By comparing the fluorescence brightness of the nanoparticle–protein complex to that of individual protein molecules, the number of bound proteins can be estimated. By adding additional non-labeled proteins to the solution one can also obtain information on the binding strength.^[8a] On the downside, care should be taken to ensure that the fluorescent labeling does not alter the protein properties in a way that may perturb interactions with the studied nanoparticles.^[91b]

In summary, the FCS technique is a powerful tool for studying protein–nanoparticle interactions. While the need for fluorescent labeling may pose some limitations, this is more than compensated for by the sensitivity and the selectivity of the technique. In perspective, FCS will probably be more often applied for studies under physiological conditions, that is, in undiluted serum or plasma and, with the recent developments of near-infrared fluorescent labels and the respective instrumentation, likely in full blood.

2.2.3. Isothermal Titration Calorimetry (ITC)

ITC is a technique designed to analyze the thermodynamic parameters of reactions or binding events and as such can be used as a complementary method to obtain similar information as with FCS. In general, the measurement principle relies on the absorption or release of heat during the interaction between two compounds. This interaction can be a chemical reaction involving the formation of covalent bonds or a non-covalent interaction such as hydrogen bonding or electrostatic forces. One compound is titrated to the other one in an isothermal environment so that heat release or absorption will result in a temperature change in the measurement cell. Consequently, the temperature will be adjusted again to match the temperature in the reference cell. The energy needed for this process gives the raw signal as an output (Figure 8, top) and can then be converted into the heat change during each titration step by integration. Additionally, for each titration, the corresponding heat of dilution (e.g., titration of protein into water or buffer) has to be determined and subtracted from the adsorption heats. The result is the so-called binding or adsorption isotherm, which can be analyzed with different mathematical models to yield the thermodynamic binding parameters (Figure 8, bottom). Originally, this method was developed to characterize mainly biomolecular processes such as enzyme–substrate interactions.^[92] This implies that optimal analysis can be provided for 1:1 interactions. However, over the last years, the application of ITC for protein adsorption measurements has become more prominent.^[93] As a characterization tool for the analysis of the processes going on when proteins interact with a specific

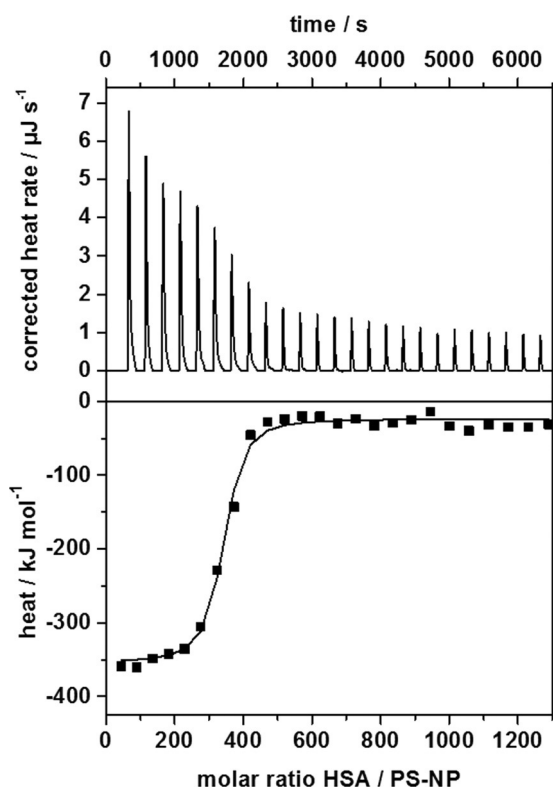


Figure 8. Typical data obtained from isothermal titration calorimetry measurements of polystyrene nanoparticles (PS-NPs) titrated with human serum albumin (HSA). Top: Corrected heat rate of the titration. Bottom: Integrated normalized heats from each titration step corrected by the heats of dilution (filled squares) together with a fit corresponding to an independent binding model (straight line).

surface, the calculated thermodynamic parameters can be extremely helpful.

Owing to the measurement principle in standard ITC devices, only solutions or suspensions can be filled into the measurement cell, which limits the method to investigations of proteins at curved surfaces/nanoparticles. With more advanced ITC devices, it is in principle possible to use cells that can be opened up so that pieces of planar substrates can be inserted. This would enable monitoring the protein adsorption also on materials other than nanocarriers as long as sufficient mixing of the solution can be ensured.

In general, three different parameters can be obtained from an adsorption experiment: the free adsorption enthalpy ΔH , the stoichiometry n of the adsorption, and the binding affinity K_a of the corresponding protein. From those parameters, the Gibbs free energy ΔG and from that entropy change ΔS as well as the heat capacity can additionally be calculated. The adsorption process can then be characterized in terms of the driving force (enthalpy vs. entropy), and the binding strengths of different proteins towards a certain nanomaterial can be compared. The determined adsorption enthalpy describes the sum of all processes requiring and releasing energy during the adsorption process. This includes electrostatic interactions, hydrogen bonds, and van der Waals forces.^[94] Thus $\Delta H < 0$ means that the adsorption process is driven by an energy gain (energy is released in the form of heat) as exemplarily shown in Figure 9 with $\Delta H \approx -300 \text{ kJ mol}^{-1}$. In contrast, the determined entropy change ΔS indicates whether the total order of the system increases or decreases. In principle, the adsorption of proteins from the solution onto a surface results in a more ordered system. However, the more hydrophobic the surface material and parts of the protein are, the more water molecules from both hydration shells will be released back into the solution, allowing for hydrophobic interactions. Accordingly, the entropy of the system increases.^[94] Importantly, this means

that from information on the driving force of the adsorption, the main interaction mechanism (enthalpy gain: electrostatic interactions; entropy gain: hydrophobic interactions) can be concluded.

The binding strength between a protein and surface is expressed by the adsorption constant K_a or its inverse, the dissociation constant K_d . The range for K_a accessible by ITC is around 10^3 – 10^9 L mol^{-1} . This means that also proteins with very low binding affinities can be detected. Thus an enormous advantage of the technique is that the soft protein corona can be analyzed. The free proteins do not have to be separated so that also the weak protein binding forces are not being disturbed. Therefore, proteins can be detected in the corona of nanocarriers that cannot be found with other techniques. Additionally, compared to FCS, none of the components need to be labeled. In some cases, however, it can happen that the protein interaction with the nanomaterial is heat-neutral at the desired temperature so that no signal can be obtained. Normally, this problem can be solved by changing the measurement temperature. However, when the adsorption parameters for a certain temperature are required, other methods have to be used to calculate adsorption isotherms. This also applies to the case when the obtained heats do not result in an adsorption isotherm with a sigmoidal curve. In that case, the data can still be fitted but the fit will result in random numbers because often no initial plateau can be found in the data.

Most of the time, the adsorption parameters are obtained from the so-called independent binding model.^[95] This binding model needs the concentrations of both interaction partners as an input so that only pure proteins—and no protein mixtures—can be analyzed. Unfortunately, sometimes the molar concentration of the nanocarriers is difficult to determine owing to polydispersity or the fact that they are hollow spheres. The model relies on the assumption that all interactions between proteins and nanomaterial are independent, meaning that already bound proteins do not change the binding affinity of the following proteins. Another assumption is that the adsorption is considered to be reversible so that the system will reach equilibrium. This might not be the case for all adsorption processes, especially when protein denaturation is involved. In addition, the model does not consider protein–protein interactions, or, in other words, it cannot describe a system where the binding affinity changes during the adsorption process. Ballauff and co-workers have developed a new model that takes those changing (or intrinsic) binding affinities into account for the interaction of proteins with hydrogel nanoparticles.^[96]

For a detailed understanding of the thermodynamic properties of a certain system, the model needs to be modified. However, this has to be done for each new system so that thus far, fast analysis is only possible with the standard data analysis models. The development of new standard models would significantly contribute to the advancement of the technique and its application for studying protein interactions with nanocarriers.

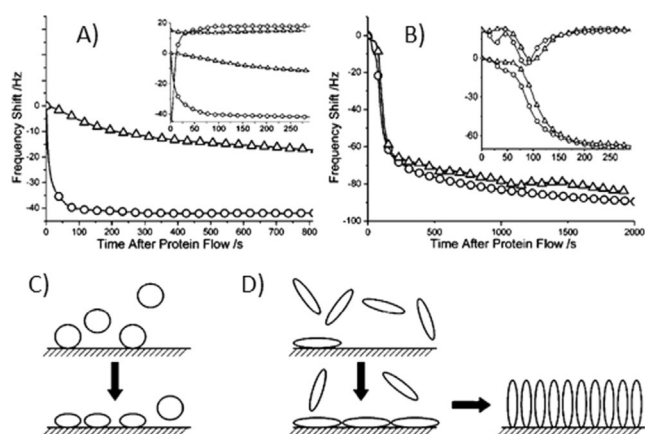


Figure 9. Adsorption profiles of A) BSA and B) fibrinogen onto CH_3 (O) and OH (Δ) terminated surfaces as measured with QCM-D. Insets show the derivative plots of the corresponding adsorption profiles. Schematic representations of C) a globular protein, such as BSA, whose conformation may change upon surface adsorption, and D) a rod-like protein, such as fibrinogen, which first adsorbs and later can rearrange to increase protein–protein interactions and the surface density of the protein. Figure adapted from Ref. [99a].

2.2.4. Quartz Crystal Microbalance with Dissipation Monitoring (QCM-D)

QCM-D is a powerful tool to study interactions between proteins and surfaces. In QCM-D, a quartz crystal is placed between two electrodes under an alternating current, which causes the crystal to oscillate at its resonance frequency f . The resonance frequency decreases as more mass binds to the crystal surface. When the alternating current is turned off, the oscillations decay at a rate that depends on the dissipative properties of the adsorbed layer. Hence, QCM-D provides a label-free method that enables real-time monitoring of dynamic interactions between proteins and surfaces, including changes in protein conformation. The changes in frequency f and dissipation D can be fitted to obtain the hydrated mass of the adsorbed protein layer with nanogram sensitivity and the viscoelastic properties of the film, including its viscosity, density, and thickness.^[97] QCM-D has been used in numerous examples to investigate the protein adsorption and desorption kinetics to planar surfaces.

The fact that QCM-D is a label-free method allows for comparing the adsorption of different proteins to planar surfaces and provides an understanding of how parameters such as protein charge, molecular weight, and buffer conditions influence the adsorbed layer.^[98] Such studies have revealed that some proteins such as BSA have quick and one-step adsorption kinetics while many extracellular matrix proteins such as fibronectin and fibrinogen display more complex adsorption behavior and undergo conformational rearrangement on the surface over time (Figure 9).^[99] On the other hand, QCM-D crystals can be flexibly modified to investigate how surface properties alter protein adsorption as well as the resulting viscoelastic consequences.^[100] For example, Hemmersam and co-workers demonstrated that fibronectin forms denser and softer films on gold surfaces than on Ti and Ta oxide.^[100b] In another study, Kushiro and co-workers revealed using QCM-D that fibronectin formed soft or rigid films depending on the functional groups on the surface and that cell adhesion to these fibronectin films did not correlate with the fibronectin surface density but with the unfolding of the protein, which exposes the RDG motif.^[99b]

The real-time monitoring provided by QCM-D allows looking at desorption and displacement kinetics in adsorbed protein layers and differentiate between reversible and irreversible binding. For instance, such studies have revealed that the unspecific binding of BSA to PEG-modified surfaces can block subsequent fibrinogen binding.^[101] Complementarily, the same study revealed that BSA can remove some unspecifically bound fibrinogen from PEG-modified surfaces. This has important implications for the design of biocompatible materials towards the prevention of unwanted blood clot formation. Similarly, QCM-D studies have revealed that the mussel adhesive protein mpf-3 can increase the adsorption of collagen type-1 on TiO₂ surfaces, which can potentially increase their biocompatibility.^[102]

QCM-D, which gives the hydrated mass in the adsorbed layer and its viscoelastic properties, can be used in combination with other techniques such as ellipsometry and surface plasmon resonance (SPR), which measure the dry mass of the adsorbed protein film. These complementary parameters are in particular useful to investigate the hydration of adsorbed proteins films and conformational changes in them upon reactions in these films such as cross-linking. Höök and co-workers revealed in a time-resolved adsorption study of the mussel adhesive protein mepf-1 with QCM-D, SPR, and ellipsometry that upon adsorption, a 20 nm thick extended highly hydrated film is formed. Upon cross-linking with NaIO₄, the protein film collapsed to 5 nm and became more compact and less water-rich, while the dry mass increased slightly.^[103] Overall, these examples illustrate that QCM-D provides unique insight into protein adsorption, desorption, and conformational changes on planar surfaces and can quantify the hydrated mass and viscoelastic properties of the protein layer in a label-free manner.

2.3. Multiscale Simulations of Protein Folding at an Interface

Particle-based computer simulations offer unique insight into the molecular mechanisms associated with complex phenomena such as proteins adsorbing at an interface. The complexity of many biomolecular systems strongly limits the capabilities of all-atom simulations—in which all atoms are

Table 2: Overview of methods also used for characterizing low-affinity proteins.

Method	Utilized protein sources	Available information
Dynamic light scattering (DLS)	Protein mixtures/ single proteins	Size (changes)/ aggregation detection/ intensity fractions
Fluorescence correlation spectroscopy (FCS)	Protein mixtures/ single proteins	Size (changes)/ concentration determination, stoichiometry/ binding affinity
Isothermal titration calorimetry (ITC)	Single proteins	Protein binding affinity/stoichiometry/ interaction driving forces (enthalpy and entropy contribution)
Quartz crystal microbalance with dissipation monitoring (QCM-D)	Protein mixtures/ single proteins	Hydrated mass of protein films, properties of viscoelastic protein films

explicitly represented—even with today's computational standards. As an example, protein folding simulations, which require significant structural rearrangements of both the protein and its environment, are notoriously demanding. Coarse-grained models lump several atoms into one larger particle or bead and thereby provide significant computational speedup, owing to a smoother energy landscape, at the expense of reduced chemical detail.^[104] Regarding the description of protein–interface interactions, certain coarse-grained models aim at modelling structure formation: Given an amino acid sequence, the environment, and the thermodynamic state point, which conformations will be sampled (e.g., α -helix, β -sheet, or random coil)? The exact folding of the protein chain into the correct major conformations requires a coarse-grained model that captures the essential physics governing the free-energy landscape of the system. A few models have demonstrated the ability to fold simple sequences without prior information about the native state.^[105]

The presence of an interface compounds the computational challenge of equilibrating the system, making coarse-grained models all the more appealing. A small number of models have tackled proteins at an interface, most of them focusing on lipid membranes. For instance, the coarse-grained peptide-lipid PLUM model is capable of stabilizing small model transmembrane helices, and reproduce not only structural features (e.g., tilt angle), but also thermodynamic aspects.^[106] The model has also been shown to be capable of folding simple sequences in the membrane, such as a two-helix-forming peptide from a bacteriophage, in good agreement with NMR experiments.^[107] Interestingly, folding in the aqueous environment predicts a very different fold: a three-helix bundle. The different folds illustrate that the model is capable of stabilizing different structures in different environments. As a result, it is capable of providing insight into protein structure and stability close to an interface. Another approach that can be easily extended to proteins at interfaces combines all atom- and particle-based coarse-grained regions with an elastic network description of the overall protein within one simulation setup.^[108]

3. Current Advances and Challenges: From Unspecific to Specific Interactions

3.1. Suppressing the Interactions between Proteins and Surfaces

The increased number of biomedical devices employed (e.g., prosthetic implants, heart stents, pacemakers, central valves, urinary catheters, sensors) has benefited human life quality and duration. An interface between the biological fluids and synthetic surfaces exhibiting higher free Gibbs energy is formed, thus thermodynamically there is a tendency for molecules such as proteins to adsorb to these devices.^[109] Nonspecific adsorption of proteins yields a loss in diagnostic tool sensitivity, platelet activation, and thrombus formation,^[110] or even leads to the generation of bacterial biofilms.^[111] Such biofilms determine not only the failure of systems but also the concomitance of nosocomial infections and deaths.^[112]

Interactions between the host body and inserted devices are complex and dynamic processes mediated through hydrogen bonding, van der Waals forces, and hydrophobic and electrostatic interactions.^[99a,110,113] In the design of biocompatible materials resisting biofouling, the adsorption process needs to be understood, and thus the biomatter (structure, size) as well as the surface characteristics (chemistry, charge, topography, and wettability) shall be considered. As reviewed by Song and Mano, the wetting characteristics of surfaces play a key role.^[113b] Immobilizing hydrophilic or amphiphilic polymers is a commonly used method. In the first group, the gold standard is poly(ethylene glycol) (PEG), while in the second we can find poly(zwitterions). Both approaches base their action on the formation of a strongly adhered hydration layer that exerts steric repulsion against proteins or cells. Unfortunately, both polymers can undergo oxidation, leading to a decrease in efficiency.^[4,114]

A promising route to hinder protein adsorption relies on the use of superhydrophobic surfaces. Motivated by the Lotus leaf effect, roughening a low-surface-energy material promotes the entrapment of air between protrusions in the so-called Cassie–Baxter wetting state (Figure 10).^[115] This reduces the interfacial contact area between a drop and the surface and facilitates the removal of eventually adsorbed proteins, microorganisms, or pollutants by the mobile drops.

Yet, there is still no common agreement on the role of surface roughness and periodicity. Hochbaum and Aizenberg presented a study on surface topography impact on *Pseudomonas aeruginosa* ordering using patterns with a similar length scale to that of the bacterial cells.^[116] Upon changing the chemistry, mechanical properties, and characteristic

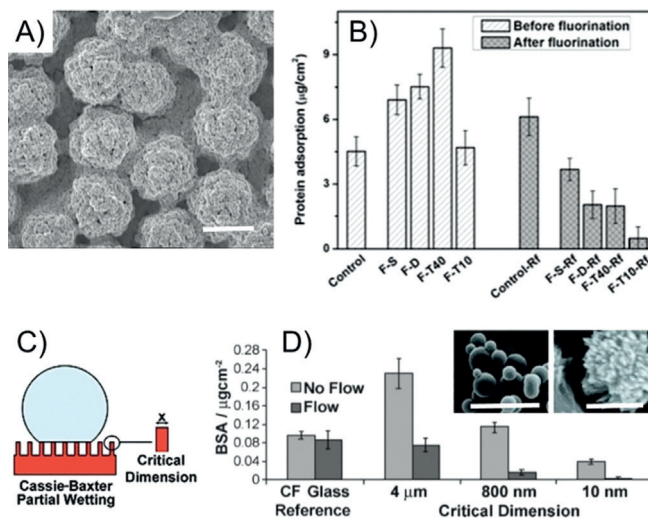


Figure 10. A) SEM image of triple-scaled surfaces (scale bar: 1 μm). B) Protein adsorption on smooth control, single (-S), dual (-D), and triple scaled (-T10, -T40, corresponding to the size of nanometric silica particles) structured surfaces before and after (-Rf) fluorination. Figure extracted and adapted from Ref. [120a]. C) Sketch of the defined critical dimension to achieve the Cassie–Baxter state. D) Protein adsorption results for fluorocarbon-terminated superhydrophobic surfaces under static and flow conditions. SEM images of micro- and nanometer patterns are shown as insets (scale bars: 10 μm and 800 nm, respectively). Extracted and adapted from Ref. [121].

length scales (size, pitch, periodicity, symmetry), the interactions between the bacteria and the surface significantly changed. Furthermore, Scopelliti and co-workers prepared nanostructured titanium surfaces to evaluate fibrinogen, bovine serum albumin (BSA), and streptavidin adsorption by fluorescence photobleaching quantification.^[117] The authors concluded that the nanoscale morphology and pore distribution of biomaterials can control the amount of adsorbed protein as they can nucleate in pores exceeding a certain aspect ratio threshold. In another work, Cai and co-workers used nanoscale titanium films prepared by electron beam evaporation (surface roughness varying from 1.9 up to 224.9 nm depending on the evaporation rate) to check BSA and human serum fibrinogen adsorption after 30 min of incubation, as well as osteoblast cell proliferation.^[118] Their results revealed little effect of roughness, in contrast to the findings of Galli and co-workers, who reported a dependence of protein A, immunoglobulin G, and F-actin adsorption on silicon and titanium nanostructures.^[119]

Zhao et al. fabricated superhydrophobic surfaces by layer-by-layer deposition of raspberry-like hydrophobized silica particles with a hierarchy of single, dual, and triple roughness (Figure 10A).^[120] Non-specific adsorption of a 1 mg mL⁻¹ solution of bovine serum albumin (BSA) incubated for 1 h was evaluated through the bicinchoninic acid (BCA) assay, showing a decrease in adsorption of up to 90% (Figure 10B). To extend the study to physiological flow conditions, Koc and co-workers evaluated the adsorption of a 3 mg mL⁻¹ BSA solution onto superhydrophobic surfaces in a fluorimetric assay (Figure 10C,D).^[121] The authors studied the effect of roughness (smooth, micro-, and nanoscale) and chemistry (hydrocarbon- and fluorocarbon-terminated) on protein adsorption after 1 h of incubation. The effect of shear forces on protein desorption was determined by subsequent flushing with buffer solution at a flow rate of 20 mL min⁻¹. The results showed that superhydrophobicity did not completely suppress protein adsorption (Figure 10D). However, under flow conditions, the amount of adsorbed protein was close to the technique detection limit. This fact indicates that the water-repellent wetting state reduces the binding strength of proteins on surfaces to such an extent that low shear forces can be sufficient to induce desorption.

In the design of biomaterials in contact with blood, platelet activation and clotting mediated through pre-adsorbed proteins should be considered. Sun and co-workers developed water-repellent surfaces made out of carbon nanotubes, observing lower platelet adhesion.^[122] Going a step further, Paven and co-workers coated metallic meshes with a superamphiphobic (i.e., repelling water and low-surface-tension liquids) candle-soot-based coating for blood-compatible materials.^[123] The coating presents a fractal-like structure made out of nanosized silica beads functionalized with a perfluorosilane. In this first study, the superamphiphobic materials were found to be low-fouling, showing protein concentrations in the range of $\mu\text{g cm}^{-2}$, the detection limit of the employed colorimetric Pierce-660 assay. Unlike plain metallic mesh immersed into blood, no adsorption of proteins or cells was observed by scanning electron microscopy. Still, fibrinogen concentrations of 5–10 ng cm⁻² can

already trigger platelet activation.^[124] Thus, for a biomaterial to be considered non-fouling, lower limits should be accomplished.

We therefore recently determined BSA and human serum concentrations on smooth, micro-, and nanoscaled silica surfaces by means of surface-sensitive and label-free X-ray photoelectron spectroscopy (XPS) and time-of-flight secondary ion mass spectrometry (ToF-SIMS) techniques.^[60c] Importantly, protein adsorption might reduce the liquid repellency of surfaces. In the worst case, superhydrophobicity might break down, resulting in complete wetting of the surface by the protein solution. Loss of superhydrophobicity increases the contact area, favoring binding of the proteins to the surface. To investigate the effect of time on protein adsorption, we exposed the samples to a 1 mg mL⁻¹ BSA solution for 2 or 24 h, which is much longer than in previous experiments and represents the time required to start adsorption kinetics of proteins at such concentration. After rinsing with a buffer solution, the level of proteins on the superamphiphobic coatings (Figure 11B), calculated through the N1s photopeak, was set below the detection limit of 2 ng cm⁻² (Figure 11C). We performed a comparison with superhydrophobic surfaces, possessing hydrophilic top faces and hydrophobic side walls (Janus pillars,^[125] Figure 11B). The protein solution partially rests on the top faces and partially on the air cushions formed between the pillars. The larger top faces allowed for protein adsorption, and thus nitrogen was detected (Figure 11C). These data suggests that super-protein repellency arises from the coupled effect of nanofeatures (reducing accessible areas) and the mobile air cushion between protein solution and solid surface (Figure 11D,E).

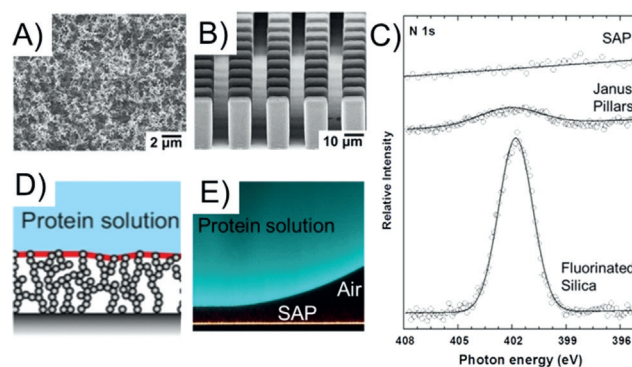


Figure 11. SEM images of liquid-repellent A) superamphiphobic and B) amphiphilic Janus pillars. C) Emission peak of nitrogen centered at 402 eV. D) Interaction of a protein aqueous solution with a superamphiphobic coating preserving a mobile air layer, as confirmed by E) laser scanning confocal microscopy. Extracted and adapted from Ref. [60c].

3.2. Control of Protein Binding through External Stimuli

Controlling protein adsorption to surfaces through changes in the environmental conditions such as temperature, pH, and light is an aspect of strong research activity. It has important implications in the areas of drug delivery, biosens-

ing, and cell–material interactions. Many efforts have concentrated on the development of smart materials that respond to external stimuli for the controlled release of proteins, specific protein immobilization, and the micropatterning of proteins.

In an early report, a pH-responsive poly(acrylic acid) (PAA) layer was used to control the adsorption of cytochrome *c*.^[126] Changing the pH resulted in a change in the electrostatic interactions between PAA and cytochrome *c*, which affected the extent of protein adsorption on PAA brushes. Not only PAA but also other polyelectrolyte brushes were used for pH-controlled protein adsorption.^[127]

Temperature-responsive materials such as PNIPAM were also used to control protein adsorption. Jiang and co-workers used temperature-responsive PNIPAM-grafted surfaces to control the adsorption of BSA with temperature. At temperatures above the LCST, the grafted layer dehydrates and shrinks, and BSA can bind through hydrophobic interactions. Upon cooling, the grafted PNIPAM layer is hydrated and extended outwards, leading to the desorption of BSA. Further modifications of BSA with cell adhesion molecules in this setup were subsequently used to control cell attachment and detachment with temperature.^[128] Similarly, temperature-sensitive PEG films were used to modulate biotin exposure in the film and the binding of streptavidin to biotin with temperature.^[129]

Light-responsive surfaces are particularly attractive for precise control over protein adsorption because they provide high spatiotemporal resolution. Therefore, light-controlled protein interactions have been particularly useful for the photopatterning of proteins into micropatterns. Photosensitive molecule classes that have been employed to construct photosensitive surfaces are azobenzene, *o*-nitrobenzil derivatives, photoswitchable proteins, and ruthenium complexes.

Azobenzenes, which reversibly isomerize between the *trans* and *cis* forms upon illumination with UV and visible light, can be used to alter surface priorities. Zhang and co-workers used this concept to alter the adsorption of BSA to multilayer azobenzene films and found that more BSA adsorbed on the *trans* film than on the *cis* film.^[130] Abell and co-workers attached an α -chymotrypsin inhibitor to an azobenzene-modified surface to alter protein adsorption with light.^[131] In their design, the *trans* isomer weakly binds with α -chymotrypsin while the *cis* isomer is a stronger binder of α -chymotrypsin.

Another compound group usually used for photocontrolled protein adsorption consists of *o*-nitrobenzil derivatives. Complementary to the approaches that rely on nonspecific interactions between proteins and substrates, many of these rely on specific interactions between proteins and substrates. In general, these are based on photocleavable caging groups such as nitrobenzyl, 3,5-dimethoxybenzoin esters, and nitro-dibenzofuran, which at first block interactions and later can be removed upon illumination to restore activity.^[132] Thus far, glutathione and biotin have been caged with photocleavable groups to control the interaction with GST-tagged and streptavidin-tagged proteins, respectively.^[133] Additionally, the Ni²⁺-mediated interaction between polyhistidine-tagged

(His-tagged) proteins and nitrilotriacetic acid (NTA) has been transformed into a light-dependent interaction either by incorporating a photocleavable amino acid into the His tag or by introducing a photocleavable functional group between the NTA and the substrate.^[134] The light-activated interaction between His-tagged proteins and Ni²⁺-NTA groups has been used to orthogonally micropattern multiple proteins by sequentially illuminating different areas and combining this interaction with other specific protein–protein interactions.^[135]

The above-mentioned systems use UV light to control protein adsorption. UV light is problematic for biomedical applications because it may cause protein damage and it cannot penetrate deeply into tissue. To overcome these problems, upconverting nanoparticles and photoswitchable proteins have been used to fabricate substrates for photocontrolled protein binding. Upconverting nanoparticles can convert near-infrared light into UV or visible light, which can induce photoreactions of conventional photosensitive compounds (Figure 12).^[136] Proteins are linked to an upconverting-nanoparticle-decorated substrate via blue-light-cleavable Ru complexes. When the substrate is irradiated with NIR light under a photomask, upconverting nanoparticles convert the NIR light into blue light in the exposed areas. This induces cleavage of the Ru complexes and release of the proteins. Photon upconversion lithography could be an approach for the patterning of biomaterials other than proteins. We envision using photon upconversion lithography to fabricate

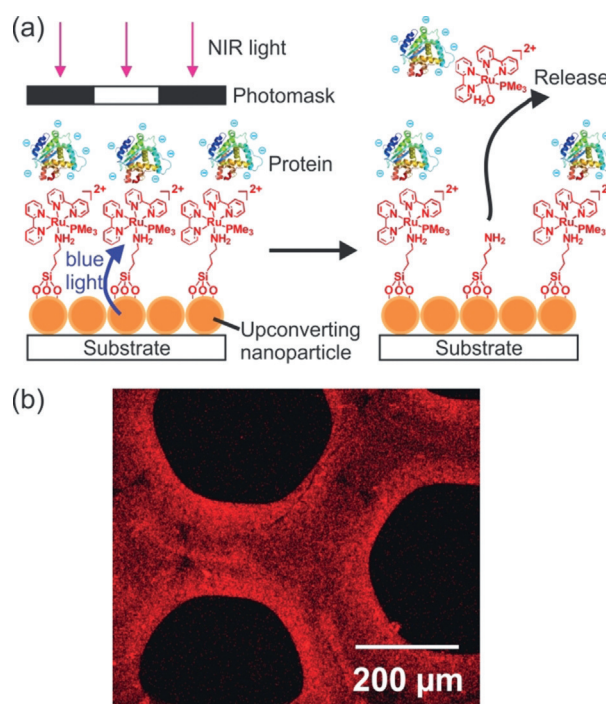


Figure 12. a) Schematic representation of photon upconversion lithography (PUCL) for the patterning of proteins. Note: Poly(ethylene glycol), co-grafted with Ru complexes on the upconverting nanoparticles (UCNPs), is not shown for clarity. b) Confocal laser scanning microscopy image of a protein pattern fabricated using PUCL. Reproduced with permission from Ref. [136]. Copyright 2015, Wiley-VCH Verlag GmbH & Co. KGaA.

patterned extracellular matrices, control the migration of cells, and guide the development of neurons. More recently, the blue-light-dependent interaction between the proteins iLID and Nano has been used to photopattern proteins on membranes.^[137] In this approach, one of the interaction partners, iLID, was anchored to the membrane so that a Nano-fused protein of interest could be specifically recruited under noninvasive low-intensity blue light. As the iLID–Nano interaction is reversed in the dark, these protein patterns are reversible and dynamic, capturing key features of protein patterns in nature.

3.3. Understanding and Predicting the Specificity of the Protein Corona around Nanocarriers

Up to several hundred proteins can be identified in the protein corona of nanoparticles by proteomics based on liquid chromatography coupled to mass spectrometry (LC-MS).^[138] It can be calculated that the less abundant ones in these lists are not even present on every nanoparticle. Therefore, the race for longer lists of proteins is not going to progress our understanding of the protein corona. Even when the lists of identified proteins are shortened to the most relevant ones, the lists still remain complex.^[13] The different proteins involved appear to be unspecifically adsorbed, but clearly they are not present at random. The same proteins will be identified on the same nanocarriers when the experiment is repeated. Small changes in the nanoparticle surface, such as the presence of traces of surfactants, can widely influence the protein corona.^[139] Therefore the notion of “unspecific” versus “specific” is more about the lack of understanding of the pattern of proteins attracted and the consequences for colloidal stability,^[84] biodistribution,^[140] and intracellular uptake and trafficking.^[141] The protein coat of a given nanoparticle is specific to it even if we did not intend it and if we cannot fully control it yet.

We are just starting to predict the proteins adsorbed and consequently the biological impacts.^[142] Here, nanocarriers with one highly predominant protein help to gain a first understanding. This has recently been demonstrated for explaining the “stealth effect”. Nanocarriers as well as technical surfaces are readily recognized by the immune system as proteins such as immunoglobulins or complement factors adsorb to these surfaces. Then immune cells try to eliminate these marked foreign substances. Modifications of surfaces have been established that do not result in immune recognition by these mechanisms—this has been termed the “stealth effect/property”.^[143] Poly(ethylene glycol) (PEG) has been the prototype of these surface modifications. Anti-fouling, protein-repellent, and anti-uptake properties were attributed to PEG as a coating material.^[144] For decades, the mere reduction in the total amount of adsorbed protein was thought to be the decisive feature. We then found that for nanoparticle surfaces with a PEG modification, one specific protein is highly predominant when exposed to blood plasma: Clusterin, also known as apolipoprotein J, was found to make up up to 70 % of the total protein content in the hard corona of these nanoparticles.^[13] These findings showed that neither

is PEG completely protein-repellent nor does PEG itself hide nanocarriers from the phagocytotic cells in the body. Based on this insight, the adsorbed clusterin is likely to be responsible for the stealth effect. In addition, this is the reason why other materials with a suspected stealth effect can now be screened, and proteins such as apolipoprotein AI or AIV have been found to be also responsible for a stealth effect and can substitute clusterin in its function.^[13] Additionally, by varying the chemical structure of the polymers used for stealth functionalization, it was shown that the hydrophilicity of the chains (and thus the material available for interaction) plays a key role in mediating the specific enrichment of stealth proteins: The higher the polymer hydrophilicity, the more clusterin and apo A I proteins were found in the corona.^[145]

With these results, computer simulations can be used to understand the molecular interaction of PEG with clusterin and other proteins.^[142] Hereby, the list of adsorbed proteins can be correctly predicted. We should keep in mind that the proteins adsorbed probably attract secondary proteins, which interact with the previously adsorbed layer.^[146] Such theoretical interaction analyses will also help to understand and dissect the more loosely bound proteins of the soft corona, for which the interaction with the first protein coat—the hard corona—is probably more important.

It is also conceivable that denaturation plays an important role for adsorption and whether the decorated surfaces are then recognized as foreign: On the one hand, for many surfaces, hydrophobic interactions are predominating the adsorption effect as described above (see ITC). As proteins usually cover up their hydrophobic parts inside the 3D structure of the folded protein, such an interaction changes the whole tertiary structure and therefore exposes the hydrophobic regions of the protein to the outside. This will also promote the recognition of the decorated surfaces as foreign. On the other hand, stealth-like polymers and surfaces will probably interact with the proteins through van der Waals forces, electrostatic interactions, and hydrogen bonds. This will less likely result in the unfolding of the protein and therefore will reduce the immune recognition. Protein denaturation will also determine whether the adsorption process itself is reversible. If significant structural changes are involved, this usually results in irreversible binding. For only slight changes, proteins might be able to fold back so that the adsorption process still represents an equilibrium. As a result, the structural elements of the protein and the nanocarrier material determine whether desorption can occur in a dynamic environment such as the blood stream.

3.4. Imparting Function by Protein Corona Engineering

3.4.1. Uptake and Intracellular Trafficking: Partners for the Protein Corona on and in Cells

Ultimately, the goal of using nanocarriers in medicine is to deliver a cargo to a specific organ, cell, or even to a specific intracellular site. This is where the adsorbed proteins are most crucial, not only for hindering the uptake into the non-target cells but also for enabling transport into the desired cell types. It has been demonstrated that certain proteins can enhance

the uptake into the target cell if they are adsorbed.^[147] These identified proteins are part of a complex composition in most protein coronas. Therefore, it is still unsolved how one can assess the net effect of a given protein composition containing cellular-uptake-enhancing and uptake-inhibiting proteins.

As shown by Dawson and co-workers, the adsorbed proteins can also screen targeting moieties such as transferrin, a protein interacting with transferrin-receptor-positive cells.^[148] This shielding effect of the targeting moiety by the protein corona is clearly something that needs to be further addressed by chemical design of the nanocarrier. Enabling only the adsorption of non-interfering proteins seems to be a complex task while enabling the targeting moiety to be placed further away from the nanoparticle surface by spacers is more achievable based on available bioconjugation technologies.

Furthermore, the proteins in the protein corona interact not only with the membrane proteins of cells but are also still present in the cell inside the endosome.^[141,149] Obviously, these protein coronas also determine the intracellular fate, such as how fast nanocarriers are transported through the cell.^[150] LC-MS can also be used to identify different types of endosomes, such as early or late endosomes, or different types of lysosomes, and therefore allows elucidating the intracellular fate of nanocarriers. This revealed hitherto not well recognized intracellular compartments,^[141] which are crucial for the fate of the respective nanocarriers. In these compartments, further receptors and enzymes are recruited from the cytosol or by fusion with other compartments. These mechanisms have not yet been exploited as a way of influencing the cellular response to a nanocarrier. In the case of enzymes, these could specifically enable the escape of cargoes from the endosome in a desired state.

3.4.2. Protein Bioadhesives Stabilize Nanoparticle Sensors

The controlled adsorption of specific proteins from biological media is still in its infancy, and the findings discussed above clearly indicate the importance of proteins at interfaces and their crucial roles in dictating cellular uptake. In order to exert greater control over the interfaces and subsequent nanocarrier properties, the interaction between proteins and nanoparticle surfaces can be predefined by design through controlled protein adsorption. Various nanoparticles such as metals,^[151] semiconductors,^[152] or nanodiamonds^[153] have been stabilized by this emerging and versatile protein passivation strategy to enable *in vitro* and *in vivo* bioapplications. There are different ways to add the desired proteins as stable bioadhesives to the nanoparticles, for example, through electrostatic interactions,^[154] non-covalent interactions,^[155] or ligand–metal interactions.^[152] As proteins offer multiple carboxylic acid, amino, and thiol/disulfide groups, ligand exchange of weakly bound nanoparticle surface groups by the desired protein represents a method of choice to passivate, for example, quantum dots.^[152] Gold nanoparticles have been coated by either ligand exchange or *in situ* growth by complexing gold cations at the protein surface and subsequent reduction.^[151] In both cases, the protein serves as a bioadhesive, improving the colloidal

stability of the nanoparticles in aqueous media, which is essential for bioimaging applications. Ultrasmall and fluorescent gold nanoemitters have been obtained by nucleation and growth in the presence of HSA.^[151a,156] HSA-coated nanogold (AuNPs) emits in the NIR region with a comparatively high fluorescence quantum yield and has sufficient stability for studies inside living cells.^[151a] More recently, a chemically modified, cationic HSA derivative was obtained containing PEG polymer chains as well as multiple mitochondria-targeting, lipophilic triphenyl phosphonium groups.^[157] The triphenylphosphonium-modified protein was then applied as a protein adhesive coating to AuNPs. The photostability and limited toxicity of these markers enabled true long-lasting 3D time lapse live-cell imaging and even quantification of mitochondrial dynamics in living cells.^[158]

Nanodiamonds (NDs) represent promising bioprobes because of their tunable, intense emission, low cellular toxicity, and very high photostability.^[159] NDs with nitrogen-vacancy defects even allow for combining various imaging modes in one nanoparticle system, such as super-resolution microscopy techniques, surface-enhanced Raman scattering, or nanoscale magnetometry (the detection of very small magnetic fields at nanoscale resolution), making them unique probes for sensing their local environments.^[160] Typical preparation processes yield NDs with multiple negatively charged surface groups, which complex to positively charged proteins. The adsorption of the protein ferritin, which transports iron in many organisms, yielded one of the first ND–protein complexes (Figure 13 a).^[161] The presence of ferritin at the ND surface was detected by recording the magnetic noise of the multiple inner paramagnetic Fe³⁺ cations as a contrast mechanism, with sensitivities reaching the single-molecule detection threshold.^[151] These results pave the way to nanoparticle sensors bearing a functional protein corona that could be detected directly by a relatively simple optical readout.

Moreover, the protein shell offers customization of the particle functions through synthetic design: The adsorption of

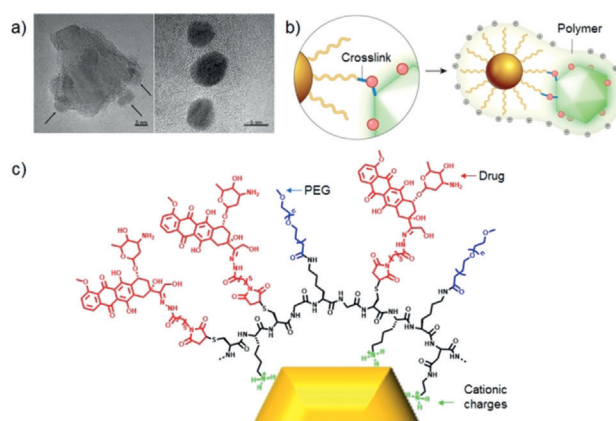


Figure 13. a) TEM image of ND with adsorbed Ferritin proteins indicated by the arrows. Magnification of three ferritin proteins adsorbed at the ND surface. b) Hybrid nanoparticle consisting of nanogold (yellow) and ND (green) obtained by covalent crosslinking of the HSA (red spheres) protein interface. Extracted and adapted from Ref. [162]. c) Multifunctional protein–particle interface obtained through chemical engineering of the protein bioadhesive.

proteins such as ferritin or HSA not only stabilizes NDs and suppresses aggregation in buffer solution but it could also serve as reactive biointerface for linking two different kinds of nanoparticles with precise structural control.^[153] The presence of multiple functionalities in the protein amino acid side chains allowed the preparation of ND–nanogold hybrid particles by covalent crosslinking of the passivating HSA layer of the NDs with the coating ligands of the nanogold (Figure 13b). Such biosensors based on multiple nanoscale components are generally challenging to obtain because of aggregation, especially in biological environments, as well as complicated purification. The ND–nanogold hybrid depicted in Figure 13b represents the first “all-in-one” hybrid particle suitable for both fluorescent imaging and electron microscopy, which enables studying cellular processes such as endocytosis, a membrane-dependent process that delivers materials to cells, in a single sample at multiple resolutions.^[153]

3.4.3. Denatured Protein Coatings for Drug Delivery and Theranostics

Proteins such as fibrinogen are known to adsorb to implanted biomaterials. Reported findings reveal that the strong adhesion is supported by denaturation of the protein structure, which in turn leads to stronger interaction with the material.^[163] Denaturation allows internal regions to form additional contacts with a particular solid surface to stabilize the interaction.^[164] Inspired by this natural adhesion process of many proteins, which efficiently passivates nanomaterials and surfaces, we have established a controlled protein denaturation and stabilization strategy that exposes functionalities that are usually “hidden” inside the protein, such as hydrophobic or thiol groups of disulfide bonds, for either introducing additional functionalities or stabilizing the nanoparticles.^[152,165] HSA was denatured and stabilized by multiple grafted PEG chains, and additional thiol groups were incorporated to encapsulate CdSe quantum dots (QDots).^[152] A reversible QD pH sensor was obtained as the emission intensity of the QDots was strongly affected by the denatured protein coating and its ability to passivate the QDot surface and adopt different charge states.^[152] By introducing multiple positive charges to denatured HSA, a QD biocoating was obtained that facilitated complex formation with DNA through electrostatic interactions. The emission intensity of the QDots depended strongly on DNA complex formation, and it even correlated with the gene transfection efficacy of the HSA–QDot complexes with DNA.^[166]

A variety of functionalities can be introduced into the protein bioadhesive by chemical modification, for example, drug molecules, DNA, polymers, or imaging groups (Figure 13c).^[167] During protein coating, these functionalities are transferred to the nanoparticle surface, which results in efficient drug transporters or nanotheranostics for cancer therapy.^[167b] Moreover, additional stabilization could be achieved by the introduction of appropriate chemical functional groups to confer better interactions with the nanoparticles. One could envision engineered multifunctional nanoparticle interfaces based on proteins encoded with

defined structural information as a convenient platform to address specific biological challenges.

4. Summary and Outlook

Specific or unspecific protein adsorption as a desired or undesired process occurs on many different surfaces and as such is very complex in nature. To be able to achieve a certain degree of control over the resulting surface characteristics, a deeper understanding of those processes is definitely required. In our opinion, it is not enough to only understand the surface activity of proteins. Rather, the aim is to create certain functions by designing a specific protein-covered or protein-repellent surface. Exploiting the surface activity of proteins should enable engineering the material characteristics directly in the applied biological environment. Gaining a fundamental understanding of protein interactions and later changes in the surrounding medium, a complementary combination of characterization techniques—possibly involving the help of computational simulations—is required. We have thus given an overview over some of the most commonly used and some of the most promising techniques. Many techniques are currently only used for the characterization of either planar or curved surfaces. However, it is also possible in some cases—and even more needed—to expand their application to the respective other material. Developing characterization methods for more universal measurement possibilities and using complementary techniques depending on the required information is mandatory. Even more, the knowledge obtained for planar surfaces needs to be translated to curved surfaces and vice versa. With those possibilities, a great step can probably be made towards engineering “functional” protein-interacting systems.

Conflict of interest

The authors declare no conflict of interest.

How to cite: *Angew. Chem. Int. Ed.* **2018**, *57*, 12626–12648
Angew. Chem. **2018**, *130*, 12806–12830

- [1] a) J. Shi, P. W. Kantoff, R. Wooster, O. C. Farokhzad, *Nat. Rev. Cancer* **2017**, *17*, 20–37; b) T. Lammers, S. Aime, W. E. Hennink, G. Storm, F. Kiessling, *Acc. Chem. Res.* **2011**, *44*, 1029–1038; c) T. L. Doane, C. Burda, *Chem. Soc. Rev.* **2012**, *41*, 2885–2911.
- [2] a) W. Norde, *Adv. Colloid Interface Sci.* **1986**, *25*, 267–340; b) S. Schöttler, K. Landfester, V. Mailänder, *Angew. Chem. Int. Ed.* **2016**, *55*, 8806–8815; *Angew. Chem.* **2016**, *128*, 8950–8959.
- [3] R. Chan, V. Chen, *J. Membr. Sci.* **2004**, *242*, 169–188.
- [4] I. Banerjee, R. C. Pangule, R. S. Kane, *Adv. Mater.* **2011**, *23*, 690–718.
- [5] P. A. Wierenga, H. Gruppen, *Curr. Opin. Colloid Interface Sci.* **2010**, *15*, 365–373.
- [6] S. Tenzer, D. Docter, S. Rosfa, A. Wlodarski, J. Kuharev, A. Rekić, S. K. Knauer, C. Bantz, T. Nawroth, C. Bier, J. Sirirattanapan, W. Mann, L. Treuel, R. Zellner, M. Maskos, H. Schild, R. H. Stauber, *ACS Nano* **2011**, *5*, 7155–7167.

- [7] S. Winzen, S. Schoettler, G. Baier, C. Rosenauer, V. Mailänder, K. Landfester, K. Mohr, *Nanoscale* **2015**, *7*, 2992–3001.
- [8] a) S. Milani, F. Baldelli Bombelli, A. S. Pitek, K. A. Dawson, J. Rädler, *ACS Nano* **2012**, *6*, 2532–2541; b) C. C. Fleischer, C. K. Payne, *Acc. Chem. Res.* **2014**, *47*, 2651–2659.
- [9] a) D. Bonvin, D. Chiappe, M. Moniatte, H. Hofmann, M. Mionic Ebersold, *Analyst* **2017**, *142*, 3805; b) C. Pisani, J. C. Gaillard, C. Dorandeu, C. Charnay, Y. Guari, J. Chopineau, J. M. Devoisselle, J. Armengaud, O. Prat, *Nanoscale* **2017**, *9*, 5769–5772.
- [10] W. Liu, J. Rose, S. Plantevin, M. Auffan, J.-Y. Bottero, C. Vidaud, *Nanoscale* **2013**, *5*, 1658–1668.
- [11] a) B. J. Olson, *Curr. Protocols Pharmacol.* **2016**, *73*, A.3a.1–a.3a.32; b) J. E. Noble, A. E. Knight, A. J. Reason, A. Di Matola, M. J. Bailey, *Mol. Biotechnol.* **2007**, *37*, 99–111.
- [12] D. Docter, U. Distler, W. Storck, J. Kuharev, D. Wunsch, A. Hahlbrock, S. K. Knauer, S. Tenzer, R. H. Stauber, *Nat. Protoc.* **2014**, *9*, 2030–2044.
- [13] S. Schöttler, G. Becker, S. Winzen, T. Steinbach, K. Mohr, K. Landfester, V. Mailänder, F. R. Wurm, *Nat. Nanotechnol.* **2016**, *11*, 372–377.
- [14] S. V. Pande, M. S. Murthy, *Anal. Biochem.* **1994**, *220*, 424–426.
- [15] O. H. Lowry, N. J. Rosebrough, A. L. Farr, R. J. Randall, *J. Biol. Chem.* **1951**, *193*, 265–275.
- [16] M. M. Bradford, *Anal. Biochem.* **1976**, *72*, 248–254.
- [17] P. K. Smith, R. I. Krohn, G. T. Hermanson, A. K. Mallia, F. H. Gartner, M. D. Provenzano, E. K. Fujimoto, N. M. Goeke, B. J. Olson, D. C. Klenk, *Anal. Biochem.* **1985**, *150*, 76–85.
- [18] U. K. Laemmli, *Nature* **1970**, *227*, 680–685.
- [19] S. F. De St. Groth, R. G. Webster, A. Datyner, *Biochim. Biophys. Acta* **1963**, *71*, 377–391.
- [20] L. J. Jones, R. P. Haugland, V. L. Singer, *Biotechniques* **2003**, *34*, 850–861.
- [21] R. C. Switzer, C. R. Merrill, S. Shifrin, *Anal. Biochem.* **1979**, *98*, 231–237.
- [22] a) W. N. Burnette, *Anal. Biochem.* **1981**, *112*, 195–203; b) H. Towbin, T. Staehelin, J. Gordon, *Proc. Natl. Acad. Sci. USA* **1979**, *76*, 4350–4354.
- [23] Z. L. Awdeh, A. R. Williamson, B. A. Askonas, *Nature* **1968**, *219*, 66–67.
- [24] P. H. O'Farrell, *J. Biol. Chem.* **1975**, *250*, 4007–4021.
- [25] M. Manfredi, E. Robotti, E. Marengo, *Methods Mol. Biol.* **2016**, *1384*, 119–154.
- [26] M. Traini, A. A. Gooley, K. Ou, M. R. Wilkins, L. Tonella, J. C. Sanchez, D. F. Hochstrasser, K. L. Williams, *Electrophoresis* **1998**, *19*, 1941–1949.
- [27] F. E. Ahmed, *Expert Rev. Proteomics* **2008**, *5*, 841–864.
- [28] E. C. Huang, J. D. Henion, *J. Am. Soc. Mass Spectrom.* **1990**, *1*, 158–165.
- [29] D. Qi, P. Brownridge, D. Xia, K. Mackay, F. F. Gonzalez-Galarza, J. Kenyani, V. Harman, R. J. Beynon, A. R. Jones, *OMICS* **2012**, *16*, 489–495.
- [30] a) C. Lindemann, N. Thomaneck, F. Hundt, T. Lerari, H. E. Meyer, D. Wolters, K. Marcus, *Biol. Chem.* **2017**, *398*, 687–699; b) U. Distler, J. Kuharev, P. Navarro, S. Tenzer, *Nat. Protoc.* **2016**, *11*, 795–812.
- [31] S. Schöttler, K. Klein, K. Landfester, V. Mailänder, *Nanoscale* **2016**, *8*, 5526–5536.
- [32] a) Y. R. Shen, *The principles of nonlinear optics*, Wiley-Interscience, Hoboken, **2003**; b) R. W. Boyd, *Nonlinear optics*, 3rd ed., Academic Press, Amsterdam, Boston, **2008**.
- [33] G. Gonella, C. Lütgebaucks, A. G. F. de Beer, S. Roke, *J. Phys. Chem. C* **2016**, *120*, 9165–9173.
- [34] S. Roke, G. Gonella, *Annu. Rev. Phys. Chem.* **2012**, *63*, 353–378.
- [35] G. Gonella, W. Gan, B. Xu, H.-L. Dai, *J. Phys. Chem. Lett.* **2012**, *3*, 2877–2881.
- [36] a) S. Ong, X. Zhao, K. B. Eisenthal, *Chem. Phys. Lett.* **1992**, *191*, 327–335; b) E. C. Y. Yan, Y. Liu, K. B. Eisenthal, *J. Phys. Chem. B* **1998**, *102*, 6331–6336; c) C. Lütgebaucks, G. Gonella, S. Roke, *Phys. Rev. B* **2016**, *94*, 195410.
- [37] J. Rinuy, P. F. Brevet, H. H. Girault, *Biophys. J.* **1999**, *77*, 3350–3355.
- [38] M. A. Kriech, J. C. Conboy, *J. Am. Chem. Soc.* **2003**, *125*, 1148–1149.
- [39] a) L. M. Hauptert, G. J. Simpson, *Annu. Rev. Phys. Chem.* **2009**, *60*, 345–365; b) B. Braunschweig, P. Mukherjee, R. B. Kutz, A. Rumpel, K. Engelhardt, W. Peukert, D. D. Dlott, A. Wieckowski in *Vibrational Spectroscopy at Electrified Interfaces* (Eds.: A. Wieckowski, C. Korzeniewski, B. Braunschweig), Wiley, Hoboken, **2013**; c) T. Weidner, D. G. Castner, *Phys. Chem. Chem. Phys.* **2013**, *15*, 12516–12524; d) S. Roy, P. A. Covert, W. R. FitzGerald, D. K. Hore, *Chem. Rev.* **2014**, *114*, 8388–8415; e) E. C. Y. Yan, L. Fu, Z. Wang, W. Liu, *Chem. Rev.* **2014**, *114*, 8471–8498; f) B. Ding, J. Jasensky, Y. Li, Z. Chen, *Acc. Chem. Res.* **2016**, *49*, 1149–1157.
- [40] V. Vogel, B. L. Smiley, *Proc. SPIE* **1993**, *1922*, pp. 86–93.
- [41] M. R. Watry, G. L. Richmond, *J. Phys. Chem. B* **2002**, *106*, 12517–12523.
- [42] J. Kim, P. S. Cremer, *ChemPhysChem* **2001**, *2*, 543–546.
- [43] a) N. T. Samuel, University of Washington, **2005**; b) O. Mermut, D. C. Phillips, R. L. York, K. R. McCrea, R. S. Ward, G. A. Somorjai, *J. Am. Chem. Soc.* **2006**, *128*, 3598–3607.
- [44] L. Schmäser, S. Roeters, H. Lutz, S. Woutersen, M. Bonn, T. Weidner, *J. Phys. Chem. Lett.* **2017**, *8*, 3101–3105.
- [45] T. Weidner, M. Dubey, N. F. Breen, J. Ash, J. E. Baio, C. Jaye, D. A. Fischer, G. P. Drobny, D. G. Castner, *J. Am. Chem. Soc.* **2012**, *134*, 8750–8753.
- [46] T. Weidner, N. F. Breen, K. Li, G. P. Drobny, D. G. Castner, *Proc. Natl. Acad. Sci. USA* **2010**, *107*, 13288–13293.
- [47] J. Wang, M. A. Even, X. Chen, A. H. Schmaier, J. H. Waite, Z. Chen, *J. Am. Chem. Soc.* **2003**, *125*, 9914–9915.
- [48] L. Fu, J. Liu, E. C. Y. Yan, *J. Am. Chem. Soc.* **2011**, *133*, 8094–8097.
- [49] S. Ye, H. Li, W. Yang, Y. Luo, *J. Am. Chem. Soc.* **2014**, *136*, 1206–1209.
- [50] a) K. T. Nguyen, S. V. Le Clair, S. Ye, Z. Chen, *J. Phys. Chem. B* **2009**, *113*, 12169–12180; b) K. T. Nguyen, J. T. King, Z. Chen, *J. Phys. Chem. B* **2010**, *114*, 8291–8300; c) P. Yang, A. Boughton, K. T. Homan, J. J. G. Tesmer, Z. Chen, *J. Am. Chem. Soc.* **2013**, *135*, 5044–5051.
- [51] a) J. M. Perry, A. J. Moad, N. J. Begue, R. D. Wampler, G. J. Simpson, *J. Phys. Chem. B* **2005**, *109*, 20009–20026; b) L. Wang, C. T. Middleton, M. T. Zanni, J. L. Skinner, *J. Phys. Chem. B* **2011**, *115*, 3713–3724; c) S. J. Roeters, C. N. van Dijk, A. Torres-Knoop, E. H. G. Backus, R. K. Campen, M. Bonn, S. Woutersen, *J. Phys. Chem. A* **2013**, *117*, 6311–6322.
- [52] R. Hennig, J. Heidrich, M. Saur, L. Schmäser, S. J. Roeters, N. Hellmann, S. Woutersen, M. Bonn, T. Weidner, J. Markl, D. Schneider, *Nat. Commun.* **2015**, *6*, 7018.
- [53] a) M. A. Donovan, Y. Y. Yimer, J. Pfaendtner, E. H. G. Backus, M. Bonn, T. Weidner, *J. Am. Chem. Soc.* **2016**, *138*, 5226–5229; b) M. A. Donovan, H. Lutz, Y. Y. Yimer, J. Pfaendtner, M. Bonn, T. Weidner, *Phys. Chem. Chem. Phys.* **2017**, *19*, 28507–28511.
- [54] R. Pandey, K. Usui, R. A. Livingstone, S. A. Fischer, J. Pfaendtner, E. H. G. Backus, Y. Nagata, J. Fröhlich-Nowoisky, L. Schmäser, S. Mauri, J. F. Scheel, D. A. Knopf, U. Pöschl, M. Bonn, T. Weidner, *Sci. Adv.* **2016**, *2*, e1501630.
- [55] G. Gonella, H. L. Dai, *Langmuir* **2014**, *30*, 2588–2599.

- [56] a) P. K. Johansson, P. Koelsch, *J. Am. Chem. Soc.* **2014**, *136*, 13598–13601; b) A. Das, A. Chakrabarti, P. K. Das, *Phys. Chem. Chem. Phys.* **2016**, *18*, 24325–24331.
- [57] J. T. Pelton, L. R. McLean, *Anal. Biochem.* **2000**, *277*, 167–176.
- [58] a) J. L. R. Arrondo, A. Muga, J. Castresana, F. M. Goñi, *Prog. Biophys. Mol. Biol.* **1993**, *59*, 23–56; b) Q. Wei, T. Becherer, S. Angioletti-Uberti, J. Dzubiella, C. Wischke, A. T. Neffe, A. Lendlein, M. Ballauff, R. Haag, *Angew. Chem. Int. Ed.* **2014**, *53*, 8004–8031; *Angew. Chem.* **2014**, *126*, 8138–8169.
- [59] J. W. C. Johnson, *Annu. Rev. Biophys. Biophys. Chem.* **1988**, *17*, 145–166.
- [60] a) R. N. Foster, E. T. Harrison, D. G. Castner, *Langmuir* **2016**, *32*, 3207–3216; b) J. E. Baio, T. Weidner, G. Interlandi, C. Mendoza-Barrera, H. E. Canavan, R. Michel, D. G. Castner, *J. Vac. Sci. Technol. B* **2011**, *29*, 04D113; c) L. Schmüser, N. Encinas, M. Paven, D. J. Graham, D. G. Castner, D. Vollmer, H. J. Butt, T. Weidner, *Biointerphases* **2016**, *11*, 031007.
- [61] S. L. McArthur, G. Mishra, C. D. Easton, in *Surface Analysis and Techniques in biology* (Ed.: V. S. Smentkowski), Springer International Publishing, Basel, **2014**, pp. 9–36.
- [62] S. Techane, D. R. Baer, D. G. Castner, *Anal. Chem.* **2011**, *83*, 6704–6712.
- [63] M. S. Wagner, S. L. McArthur, T. A. Horbett, D. G. Castner, *J. Biomater. Sci. Polym. Ed.* **2002**, *13*, 407–428.
- [64] J. Franz, D. J. Graham, L. Schmüser, J. E. Baio, M. Lelle, K. Peneva, K. Müllen, D. G. Castner, M. Bonn, T. Weidner, *Biointerphases* **2015**, *10*, 019009.
- [65] D. G. Castner, B. D. Ratner, *Surf. Sci.* **2002**, *500*, 28–60.
- [66] A. Benninghoven, *Angew. Chem. Int. Ed. Engl.* **1994**, *33*, 1023–1043; *Angew. Chem.* **1994**, *106*, 1075–1096.
- [67] D. G. Castner, *Biointerphases* **2017**, *12*, 02C301.
- [68] S. Rode, N. Oyabu, K. Kobayashi, H. Yamada, A. Kühnle, *Langmuir* **2009**, *25*, 2850–2853.
- [69] Y. Zhao, R. Berger, K. Landfester, D. Crespy, *Polym. Chem.* **2014**, *5*, 365–371.
- [70] H. J. Butt, K. H. Downing, P. K. Hansma, *Biophys. J.* **1990**, *58*, 1473–1480.
- [71] S. Husale, H. H. J. Persson, O. Sahin, *Nature* **2009**, *462*, 1075–1078.
- [72] J. Holst, S. Watson, M. S. Lord, S. S. Eamegdool, D. V. Bax, L. B. Nivison-Smith, A. Kondyurin, L. Ma, A. F. Oberhauser, A. S. Weiss, J. E. J. Rasko, *Nat. Biotechnol.* **2010**, *28*, 1123–1128.
- [73] T. A. Nick, T. E. de Oliveira, D. W. Pilat, F. Spenkuch, H.-J. Butt, M. Helm, P. A. Netz, R. Berger, *J. Phys. Chem. B* **2016**, *120*, 6479–6489.
- [74] D. J. Müller, A. Engel, *Nat. Protoc.* **2007**, *2*, 2191–2197.
- [75] J. Preiner, A. Ebner, L. Chtcheglova, R. Zhu, P. Hinterdorfer, *Nanotechnology* **2009**, *20*, 215103.
- [76] a) W. Cai, Z. Liu, Y. Chen, G. Shang, *Sci. Adv. Mater.* **2017**, *9*, 77–88; b) L. M. Picco, L. Bozec, A. Ulcinas, D. J. Engledew, M. Antognozzi, M. A. Horton, M. J. Miles, *Nanotechnology* **2007**, *18*, 044030; c) A. Rajendran, M. Endo, H. Sugiyama, *Chem. Rev.* **2014**, *114*, 1493–1520.
- [77] N. Kodera, D. Yamamoto, R. Ishikawa, T. Ando, *Nature* **2010**, *468*, 72–76.
- [78] N. S. Malvankar, S. E. Yalcin, M. T. Tuominen, D. R. Lovley, *Nat. Nano* **2014**, *9*, 1012–1017.
- [79] a) D. Song, D. Forciniti, *J. Colloid Interface Sci.* **2000**, *221*, 25–37; b) S. Zhang, Y. Moustafa, Q. Huo, *ACS Appl. Mater. Interfaces* **2014**, *6*, 21184–21192.
- [80] K. Fischer, M. Schmidt, *Biomaterials* **2016**, *98*, 79–91.
- [81] M. Cui, R. Liu, Z. Deng, G. Ge, Y. Liu, L. Xie, *Nano Res.* **2014**, *7*, 345–352.
- [82] K. Rausch, A. Reuter, K. Fischer, M. Schmidt, *Biomacromolecules* **2010**, *11*, 2836–2839.
- [83] a) B. Kang, P. Okwieka, S. Schöttler, S. Winzen, J. Langhanki, K. Mohr, T. Opatz, V. Mailänder, K. Landfester, F. R. Wurm, *Angew. Chem. Int. Ed.* **2015**, *54*, 7436–7440; *Angew. Chem.* **2015**, *127*, 7544–7548; b) L. K. Müller, J. Simon, S. Schöttler, K. Landfester, V. Mailänder, K. Mohr, *RSC Adv.* **2016**, *6*, 96495–96509.
- [84] K. Mohr, M. Sommer, G. Baier, S. Schöttler, P. Okwieka, *J. Nanomed. Nanotechnol.* **2014**, *5*, 2.
- [85] R. Rigler, E. Elson, *Fluorescence Correlation Spectroscopy: Theory and Applications*, Springer, Berlin, New York, **2001**.
- [86] a) S. A. Kim, P. Schuille, *Curr. Opin. Neurobiol.* **2003**, *13*, 583–590; b) S. T. Hess, S. Huang, A. A. Heikal, W. W. Webb, *Biochemistry* **2002**, *41*, 697–705.
- [87] a) C. M. Papadakis, P. Košovan, W. Richtering, D. Wöll, *Colloid Polym. Sci.* **2014**, *292*, 2399–2411; b) K. Koynov, H.-J. Butt, *Curr. Opin. Colloid Interface Sci.* **2012**, *17*, 377–387.
- [88] a) X. Jiang, S. Weise, M. Hafner, C. Röcker, F. Zhang, W. J. Parak, G. U. Nienhaus, *J. R. Soc. Interface* **2010**, *7*, S5–S13; b) P. Maffre, K. Nienhaus, F. Amin, W. J. Parak, G. U. Nienhaus, *Beilstein J. Nanotechnol.* **2011**, *2*, 374; c) C. Röcker, M. Pözl, F. Zhang, W. J. Parak, G. U. Nienhaus, *Nat. Nano* **2009**, *4*, 577–580; d) P. Maffre, S. Brandholt, K. Nienhaus, L. Shang, W. J. Parak, G. U. Nienhaus, *Beilstein J. Nanotechnol.* **2014**, *5*, 2036–2047.
- [89] a) I. Kohli, S. Alam, B. Patel, A. Mukhopadhyay, *Appl. Phys. Lett.* **2013**, *102*, 203705; b) S. Alam, A. Mukhopadhyay, *J. Phys. Chem. C* **2014**, *118*, 27459–27464.
- [90] H. Wang, L. Shang, P. Maffre, S. Hohmann, F. Kirschhöfer, G. Brenner-Weiß, G. U. Nienhaus, *Small* **2016**, *12*, 5836–5844.
- [91] a) C. Czeslik, R. Jansen, M. Ballauff, A. Wittemann, C. A. Royer, E. Gratton, T. Hazlett, *Phys. Rev. E* **2004**, *69*, 021401; b) S. Winzen, K. Koynov, K. Landfester, K. Mohr, *Colloids Surf. B* **2016**, *147*, 124–128.
- [92] a) R. O'Brien, I. Haq, *Biacolorimetry* **2004**, *2*, 1–34; b) M. J. Cliff, J. E. Ladbury, *J. Mol. Recognit.* **2003**, *16*, 383–391.
- [93] M. Kabiri, L. D. Unsworth, *Biomacromolecules* **2014**, *15*, 3463–3473.
- [94] W. Norde, *Macromol. Symp.* **1996**, *103*, 5–18.
- [95] a) E. Freire, O. L. Mayorga, M. Straume, *Anal. Chem.* **1990**, *62*, 950A–959A; b) E. Lewis, K. Murphy in *Protein-Ligand Interactions, Vol. 305* (Ed.: G. Ulrich Nienhaus), Humana Press, Totowa, NJ, **2005**, pp. 1–15.
- [96] a) C. Yigit, N. Welsch, M. Ballauff, J. Dzubiella, *Langmuir* **2012**, *28*, 14373–14385; b) M. Oberle, C. Yigit, S. Angioletti-Uberti, J. Dzubiella, M. Ballauff, *J. Phys. Chem. B* **2015**, *119*, 3250–3258.
- [97] a) M. Tagaya, *Polym. J.* **2015**, *47*, 599–608; b) J. L. Jordan, E. J. Fernandez, *Biotechnol. Bioeng.* **2008**, *101*, 837–842.
- [98] N. Chandrasekaran, S. Dimartino, C. J. Fee, *Chem. Eng. Res. Des.* **2013**, *91*, 1674–1683.
- [99] a) P. Roach, D. Farrar, C. C. Perry, *J. Am. Chem. Soc.* **2005**, *127*, 8168–8173; b) K. Kushihiro, C. H. Lee, M. Takai, *Biomater. Sci.* **2016**, *4*, 989–997.
- [100] a) S. M. S. Schönwälder, F. Bally, L. Heinke, C. Azucena, O. D. Bulut, S. Heissler, F. Kirschhöfer, T. P. Gebauer, A. T. Neffe, A. Lendlein, G. Brenner-Weiss, J. Lahann, A. Welle, J. Overhage, C. Wöll, *Biomacromolecules* **2014**, *15*, 2398–2406; b) A. G. Hemmersam, K. Rechendorff, M. Foss, D. S. Sutherland, F. Besenbacher, *J. Colloid Interface Sci.* **2008**, *320*, 110–116.
- [101] J. Jin, W. Jiang, J. Yin, X. Ji, P. Stagnaro, *Langmuir* **2013**, *29*, 6624–6633.
- [102] N. R. M. Rodriguez, S. Das, Y. Kaufman, W. Wei, J. N. Israelachvili, J. H. Waite, *Biomaterials* **2015**, *51*, 51–57.
- [103] F. Höök, B. Kasemo, T. Nylander, C. Fant, K. Sott, H. Elwing, *Anal. Chem.* **2001**, *73*, 5796–5804.
- [104] C. Peter, K. Kremer, *Soft Matter* **2009**, *5*, 4357–4366.

- [105] a) F. Ding, J. M. Borreguero, S. V. Buldyrey, H. E. Stanley, N. V. Dokholyan, *Proteins Struct. Funct. Bioinf.* **2003**, *53*, 220–228; b) I. Coluzza, *PLoS one* **2011**, *6*, e20853; c) P. Derreumaux, N. Mousseau, *J. Chem. Phys.* **2007**, *126*, 025101; d) T. Bereau, M. Deserno, *J. Chem. Phys.* **2009**, *130*, 235106.
- [106] T. Bereau, W. D. Bennett, J. Pfaendtner, M. Deserno, M. Karttunen, *J. Chem. Phys.* **2015**, *143*, 243127.
- [107] P. McDonnell, K. Shon, Y. Kim, S. Opella, *J. Mol. Biol.* **1993**, *233*, 447–463.
- [108] A. C. Fogarty, R. Potestio, K. Kremer, *Proteins Struct. Funct. Bioinf.* **2016**, *84*, 1902–1913.
- [109] K. Nakanishi, T. Sakiyama, K. Imamura, *J. Biosci. Bioeng.* **2001**, *91*, 233–244.
- [110] K. P. M. Amiji, *J. Biomater. Sci. Polym. Ed.* **1993**, *4*, 217–234.
- [111] B. D. Ratner, S. J. Bryant, *Annu. Rev. Biomed. Eng.* **2004**, *6*, 41–75.
- [112] a) J. Zhao, L. Song, Q. Shi, S. Luan, J. Yin, *ACS Appl. Mater. Interfaces* **2013**, *5*, 5260–5268; b) G. B. Sigal, M. Mrksich, G. M. Whitesides, *J. Am. Chem. Soc.* **1998**, *120*, 3464–3473; c) R. M. Donlan, *Clin. Infect. Dis.* **2001**, *33*, 1387–1392.
- [113] a) J. D. Andrade, V. Hlady in *Biopolymers/Non-Exclusion HPLC*, Springer, Berlin, Heidelberg, **1986**, pp. 1–63; b) W. Song, J. F. Mano, *Soft Matter* **2013**, *9*, 2985–2999; c) G. Raffaini, F. Ganazzoli, *Langmuir* **2010**, *26*, 5679–5689.
- [114] a) J. Blümmel, N. Perschmann, D. Aydin, J. Drinjakovic, T. Surrey, M. Lopez-Garcia, H. Kessler, J. P. Spatz, *Biomaterials* **2007**, *28*, 4739–4747; b) I. Izquierdo-Barba, M. Colilla, M. Vallet-Regí, *Acta Biomater.* **2016**, *40*, 201–211.
- [115] a) W. Barthlott, C. Neinhuis, *Planta* **1997**, *202*, 1–8; b) Y. Zheng, H. Bai, Z. Huang, X. Tian, F.-Q. Nie, Y. Zhao, J. Zhai, L. Jiang, *Nature* **2010**, *463*, 640–643; c) A. B. D. Cassie, S. Baxter, *Trans. Faraday Soc.* **1944**, *40*, 546–551; d) H. Y. Erbil, *Surf. Sci. Rep.* **2014**, *69*, 325–365.
- [116] A. I. Hochbaum, J. Aizenberg, *Nano Lett.* **2010**, *10*, 3717–3721.
- [117] P. E. Scopelliti, A. Borgonovo, M. Indrieri, L. Giorgetti, G. Bongiorno, R. Carbone, A. Podestà, P. Milani, *PLOS ONE* **2010**, *5*, e11862.
- [118] K. Cai, J. Bossert, K. D. Jandt, *Colloids Surf. B* **2006**, *49*, 136–144.
- [119] C. Galli, M. Collaud Coen, R. Hauert, V. L. Katanaev, P. Gröning, L. Schlapbach, *Colloids Surf. B* **2002**, *26*, 255–267.
- [120] a) J. Zhao, L. Song, J. Yin, W. Ming, *Chem. Commun.* **2013**, *49*, 9191–9193; b) W. Ming, D. Wu, R. van Benthem, G. de With, *Nano Lett.* **2005**, *5*, 2298–2301.
- [121] Y. Koc, A. J. de Mello, G. McHale, M. I. Newton, P. Roach, N. J. Shirtcliffe, *Lab Chip* **2008**, *8*, 582–586.
- [122] T. Sun, H. Tan, D. Han, Q. Fu, L. Jiang, *Small* **2005**, *1*, 959–963.
- [123] a) M. Paven, P. Papadopoulos, S. Schöttler, X. Deng, V. Mailänder, D. Vollmer, H.-J. Butt, *Nat. Commun.* **2013**, *4*, 2512; b) X. Deng, L. Mammen, H.-J. Butt, D. Vollmer, *Science* **2012**, *335*, 67.
- [124] M. C. Shen, L. Martinson, M. S. Wagner, D. G. Castner, B. D. Ratner, T. A. Horbett, *J. Biomater. Sci. Polym. Ed.* **2002**, *13*, 367–390.
- [125] L. Mammen, K. Bley, P. Papadopoulos, F. Schellenberger, N. Encinas, H.-J. Butt, C. K. Weiss, D. Vollmer, *Soft Matter* **2015**, *11*, 506–515.
- [126] J. Zhou, X. Lu, J. Hu, J. Li, *Chem. Eur. J.* **2007**, *13*, 2847–2853.
- [127] a) Q. Yu, H. Chen, Y. Zhang, L. Yuan, T. Zhao, X. Li, H. Wang, *Langmuir* **2010**, *26*, 17812–17815; b) X. Wang, R. Berger, J. I. Ramos, T. Wang, K. Koynov, G. Liu, H.-J. Butt, S. Wu, *RSC Adv.* **2014**, *4*, 45059–45064.
- [128] H. Liu, X. Liu, J. Meng, P. Zhang, G. Yang, B. Su, K. Sun, L. Chen, D. Han, S. Wang, L. Jiang, *Adv. Mater.* **2013**, *25*, 922–927.
- [129] H. M. Zareie, C. Boyer, V. Bulmus, E. Nateghi, T. P. Davis, *ACS Nano* **2008**, *2*, 757–765.
- [130] J. Zhang, T. Hu, Y. Liu, Y. Ma, J. Dong, L. Xu, Y. Zheng, H. Yang, G. Wang, *ChemPhysChem* **2012**, *13*, 2671–2675.
- [131] D. Pearson, A. D. Abell, *Chemistry* **2010**, *16*, 6983–6992.
- [132] J. Cui, V. S. Miguel, A. del Campo, *Macromol. Rapid Commun.* **2013**, *34*, 310–329.
- [133] a) V. Gatterdam, R. Ramadass, T. Stoess, M. A. Fichte, J. Wachtveitl, A. Heckel, R. Tampe, *Angew. Chem. Int. Ed.* **2014**, *53*, 5680–5684; *Angew. Chem.* **2014**, *126*, 5787–5791; b) S. A. Sundberg, R. W. Barrett, M. Pirrung, A. L. Lu, B. Kiangsootra, C. P. Holmes, *J. Am. Chem. Soc.* **1995**, *117*, 12050–12057; c) T. Terai, E. Maki, S. Sugiyama, Y. Takahashi, H. Matsumura, Y. Mori, T. Nagano, *Chem. Biol.* **2011**, *18*, 1261–1272; d) C. A. Custódio, V. San Miguel-Arranz, R. A. Gropeanu, M. Gropeanu, M. Wirkner, R. L. Reis, J. F. Mano, A. del Campo, *Langmuir* **2014**, *30*, 10066–10071.
- [134] a) S. V. Wegner, O. I. Senturk, J. P. Spatz, *Sci. Rep.* **2015**, *5*, 18309; b) M. Bhagawati, S. Lata, R. Tampe, J. Piehler, *J. Am. Chem. Soc.* **2010**, *132*, 5932–5933.
- [135] a) N. Labòria, R. Wieneke, R. Tampé, *Angew. Chem. Int. Ed.* **2013**, *52*, 848–853; *Angew. Chem.* **2013**, *125*, 880–886; b) C. Grunwald, K. Schulze, A. Reichel, V. U. Weiss, D. Blaas, J. Piehler, K.-H. Wiesmiller, R. Tampé, *Proc. Natl. Acad. Sci. USA* **2010**, *107*, 6146–6151; c) M. Gropeanu, M. Bhagawati, R. A. Gropeanu, G. M. Rodriguez Muiz, S. Sundaram, J. Piehler, A. del Campo, *Small* **2013**, *9*, 838–845.
- [136] Z. Chen, S. He, H. J. Butt, S. Wu, *Adv. Mater.* **2015**, *27*, 2203–2206.
- [137] S. M. Bartelt, E. Chervyachkova, J. Steinkühler, J. Ricken, R. Wieneke, R. Tampe, R. Dimova, S. V. Wegner, *Chem. Commun.* **2018**, *54*, 948–951.
- [138] S. Schöttler, K. Landfester, V. Mailänder, *Angew. Chem. Int. Ed.* **2016**, *55*, 8806–8815; *Angew. Chem.* **2016**, *128*, 8950–8959.
- [139] S. Winzen, J. C. Schwabacher, J. Müller, K. Landfester, K. Mohr, *Biomacromolecules* **2016**, *17*, 3845–3851.
- [140] U. Sakulku, L. Maurizi, M. Mahmoudi, M. Motazacker, M. Vries, A. Gramoun, M. G. Ollivier Beuzelin, J. P. Vallee, F. Rezaee, H. Hofmann, *Nanoscale* **2014**, *6*, 11439–11450.
- [141] D. Hofmann, S. Tenzer, M. B. Bannwarth, C. Messerschmidt, S.-F. Glaser, H. Schild, K. Landfester, V. Mailänder, *ACS Nano* **2014**, *8*, 10077–10088.
- [142] G. Settanni, J. Zhou, T. Suo, S. Schöttler, K. Landfester, F. Schmid, V. Mailänder, *Nanoscale* **2017**, *9*, 2138–2144.
- [143] F. F. Davis, *Adv. Drug Delivery Rev.* **2002**, *54*, 457–458.
- [144] U. Wattendorf, H. P. Merkle, *J. Pharm. Sci.* **2008**, *97*, 4655–4669.
- [145] J. Simon, T. Wolf, K. Klein, K. Landfester, V. Mailänder, F. R. Wurm, *Angew. Chem. Int. Ed.* **2018**, *57*, 5548–5553; *Angew. Chem.* **2018**, *130*, 5647–5653.
- [146] C. Pisani, J.-C. Gaillard, M. Odorico, J. L. Nyalosaso, C. Charnay, Y. Guari, J. Chopineau, J.-M. Devoisselle, J. Armengaud, O. Prat, *Nanoscale* **2017**, *9*, 1840–1851.
- [147] S. Ritz, S. Schöttler, N. Kotman, G. Baier, A. Musyanovych, J. Kuharev, K. Landfester, H. Schild, O. Jahn, S. Tenzer, V. Mailänder, *Biomacromolecules* **2015**, *16*, 1311–1321.
- [148] A. Salvati, A. S. Pitek, M. P. Monopoli, K. Prapainop, F. B. Bombelli, D. R. Hristov, P. M. Kelly, C. Aberg, E. Mahon, K. A. Dawson, *Nat. Nanotechnol.* **2013**, *8*, 137–143.
- [149] F. Bertoli, D. Garry, M. P. Monopoli, A. Salvati, K. A. Dawson, *ACS Nano* **2016**, *10*, 10471–10479.
- [150] a) S. Tomcin, G. Baier, K. Landfester, V. Mailänder, *Int. J. Nanomed.* **2014**, *9*, 5471–5489; b) L. Nuhn, S. Tomcin, K. Miyata, V. Mailänder, K. Landfester, K. Kataoka, R. Zentel, *Biomacromolecules* **2014**, *15*, 4111–4121.
- [151] a) J. Xie, Y. Zheng, J. Y. Ying, *J. Am. Chem. Soc.* **2009**, *131*, 888–889; b) M. Tebbe, C. Kuttner, M. Männel, A. Fery, M. Chanana, *ACS Appl. Mater. Interfaces* **2015**, *7*, 5984–5991.

- [152] Y. Wu, S. Chakraborty, R. A. Gropeanu, J. Wilhelmi, Y. Xu, K. S. Er, S. L. Kuan, K. Koynov, Y. Chan, T. Weil, *J. Am. Chem. Soc.* **2010**, *132*, 5012–5014.
- [153] W. Liu, B. Naydenov, S. Chakraborty, B. Wuensch, K. Hübner, S. Ritz, H. Cölfen, H. Barth, K. Koynov, H. Qi, R. Leiter, R. Reuter, J. Wrachtrup, F. Boldt, J. Scheuer, U. Kaiser, M. Sison, T. Lasser, P. Tinnefeld, F. Jelezko, P. Walther, Y. Wu, T. Weil, *Nano Lett.* **2016**, *16*, 6236–6244.
- [154] L. Shang, Y. Wang, J. Jiang, S. Dong, *Langmuir* **2007**, *23*, 2714–2721.
- [155] a) P. Satzer, F. Svec, G. Sekot, A. Jungbauer, *Eng. Life Sci.* **2016**, *16*, 238–246; b) Z. Aghili, S. Taheri, H. A. Zeinabad, L. Pishkar, A. A. Saboury, A. Rahimi, M. Falahati, *PLOS ONE* **2016**, *11*, e0164878.
- [156] P. Zhang, X. X. Yang, Y. Wang, N. W. Zhao, Z. H. Xiong, C. Z. Huang, *Nanoscale* **2014**, *6*, 2261–2269.
- [157] S. Chakraborty, B. K. Agrawalla, A. Stumper, N. M. Vegi, S. Fischer, C. Reichardt, M. Kögler, B. Dietzek, M. Feuring-Buske, C. Buske, S. Rau, T. Weil, *J. Am. Chem. Soc.* **2017**, *139*, 2512–2519.
- [158] M. Sison, S. Chakraborty, J. Extermann, A. Nahas, P. James Marchand, A. Lopez, T. Weil, T. Lasser, *Sci. Rep.* **2017**, *7*, 43275.
- [159] Y. Wu, F. Jelezko, M. B. Plenio, T. Weil, *Angew. Chem. Int. Ed.* **2016**, *55*, 6586–6598; *Angew. Chem.* **2016**, *128*, 6696–6709.
- [160] C. S. Wood, M. M. Stevens, *Nature* **2016**, *539*, 505–506.
- [161] A. Ermakova, G. Pramanik, J. M. Cai, G. Algara-Siller, U. Kaiser, T. Weil, Y. K. Tzeng, H. C. Chang, L. P. McGuinness, M. B. Plenio, B. Naydenov, F. Jelezko, *Nano Lett.* **2013**, *13*, 3305–3309.
- [162] N. E. L. Schmäser, M. Paven, D. G. Castner, D. Graham, D. Vollmer, H.-J. Butt, T. Weidner, *Biointerphases* **2016**, *11*, 031007.
- [163] V. Balasubramanian, N. K. Grusin, R. W. Bucher, V. T. Turitto, S. M. Slack, *J. Biomed. Mater. Res.* **1999**, *44*, 253–260.
- [164] T. A. Horbett, *Cardiovasc. Pathol.* **1993**, *2*, 137–148.
- [165] F. Liu, T. Bing, D. Shangguan, M. Zhao, N. Shao, *Anal. Chem.* **2016**, *88*, 10631–10638.
- [166] Y. Wu, K. Eisele, M. Doroshenko, G. Algara-Siller, U. Kaiser, K. Koynov, T. Weil, *Small* **2012**, *8*, 3465–3475.
- [167] a) T. Zhang, A. Neumann, J. Lindlau, Y. Wu, G. Pramanik, B. Naydenov, F. Jelezko, F. Schüder, S. Huber, M. Huber, F. Stehr, A. Högele, T. Weil, T. Liedl, *J. Am. Chem. Soc.* **2015**, *137*, 9776–9779; b) Y. Wu, A. Ermakova, W. Liu, G. Pramanik, T. M. Vu, A. Kurz, L. McGuinness, B. Naydenov, S. Hafner, R. Reuter, J. Wrachtrup, J. Isoya, C. Förtsch, H. Barth, T. Simmet, F. Jelezko, T. Weil, *Adv. Funct. Mater.* **2015**, *25*, 6576–6585.

Manuscript received: December 5, 2017

Revised manuscript received: March 13, 2018

Accepted manuscript online: April 17, 2018

Version of record online: August 30, 2018